Physiological and transcriptomic variability indicative of differences in key functions within a single coral colony

Jeana L. Drake[1+], Assaf Malik[1+], Yotam Popovits[1+], Oshra Yosef[1], Eli Shemesh[1], Jarosław Stolarski[2], Dan Tchernov[1,3], Daniel Sher[1*] and Tali Mass[1,3*]

[1]Department of Marine Biology, University of Haifa, 199 Aba Koushy Avenue, Haifa, Israel, 3498838
[2]Institute of Paleobiology, Polish Academy of Sciences, Twarda 51/55, Warsaw, Poland, 00-818
[3]Morris Kahn Marine Research Station, The Leon H. Charney School of Marine Sciences, University of Haifa, Sdot Yam, Israel

+These authors contributed equally

[*]**Corresponding authors:**
Jeana Drake (during review)
jeanadrake@g.ucla.edu
Tali Mass and Daniel Sher (for publication)
tmass@univ.haifa.ac.il, dsher@univ.haifa.ac.il

Keywords: Differential gene expression, biomineralization, toxins, host and symbiont

Abstract
Polyps in different locations on individual stony coral colonies experience variation in numerous environmental conditions including flow and light, potentially leading to transcriptional and physiological differences across the colony. Here, we describe high-resolution physiological measurements and differential gene expression from multiple locations within a single colony of *Stylophora pistillata*, aiming to relate these to environmental gradients across the coral colony. We observed broad transcriptional responses in both the host and photosymbiont in response to height above the substrate, cardinal direction, and, most strongly, location along the branch axis. Specifically, several key physiological processes in the host appear more active toward branch tips including several metabolic pathways, toxin production for prey capture or defense, and biomolecular mechanisms of biomineralization. Further, the increase in gene expression related to these processes toward branch tips is conserved between *S. pistillata* and *Acropora* spp. The photosymbiont appears to respond transcriptionally to relative light intensity along the branch and due to cardinal direction. These differential responses were observed across the colony despite its genetic homogeneity and likely inter-polyp communication. While not a classical division of labor, each part of the colony appears to have distinct functional roles related to polyps' differential exposure to environmental conditions.

1 Introduction

Coral reefs remain one of the most biodiverse ecosystems on Earth (Knowlton et al., 2010), despite facing a suite of anthropogenic stressors with both local and global causes (e.g., Hughes, 1994;Hoegh-Guldberg et al., 2019). Most stony corals (order Scleractinia), the sessile builders of the reef system, grow as colonies of thousands of genetically identical polyps formed by budding, with colonies ranging from centimeters to meters in diameter. The reef-building corals are also host to intracellular symbiotic dinoflagellates whose photosynthetic activity restricts the coral holobiont to the top ~100 m of the ocean and fulfills much of the host's carbon nutritional requirements (e.g., Falkowski et al.). Nevertheless, active feeding on particles from the water column plays a significant role as well (e.g., Martinez et al.), with active predation utilizing toxins produced and delivered by cnidocytes (recently reviewed by Schmidt et al.). These fixed carbon sources ultimately power the production of the external calcium carbonate skeleton that forms the reef and persists after the animal has died.

While the individual polyps in most colonial corals are genetically identical, each polyp inhabits a distinct location within the colony, which can be morphologically complex (e.g., in the case of branching corals). Thus, it has been suggested that individual polyps within a coral colony are differentially exposed to environmental conditions such as water flow and light availability (e.g., Carpenter and Patterson, 2007;Chang et al., 2009), which have distinct effects on coral physiology. These micro-environmental conditions may play a role in feeding capability (Sebens et al., 1997), reproductive success (Mass et al., 2011), photosynthesis (Dennison and Barnes;Mass et al., 2007), calcification rate (Dennison and Barnes, 1988), and waste removal (Mass et al., 2010). For instance, reductions in flow between the colony branches can trap food particles, making it easier for hunting tentacles of the polyps to efficiently pull them from the water column (Chang et al., 2009), and leading to downstream effects on metabolism (e.g., Gladfelter et al., 1989). Similarly, differences in light exposure due to the coral's branching leads to self-shading that can dramatically reduce light availability (Anthony et al., 2005), potentially leading to fine-scale spatial heterogeneity in photosynthetic parameters between individual polyps as well as between polyps and the coenosarc (Ralph et al., 2002). We hypothesize that such physiological differences will be underpinned by transcriptional differences. Plasticity in host gene expression has been observed at coral branch tips versus bases across multiple colonies (Hemond et al., 2014). However, it has not previously been linked, at high spatial resolution, to physiological and morphological measurements indicative of relevant environmental parameters and physiology within a single coral colony.

Here we combined high-resolution transcriptomic analysis with field measurements and physiological assays to describe intra-colony plasticity in the Indo-Pacific stony coral, *Stylophora pistillata*. We sought to answer two questions: first, are there differences in function by groups of polyps at different locations throughout the colony; and secondly, can we attribute those differences to specific location characteristics that are likely associated with varying microenvironments across the colony? Our whole-genome expression and physiological data are from a single coral colony at three locations along each branch taken from a different location within the colony. This high-resolution dataset enables us to resolve variability along three main axes – tip-junction-base, top to bottom, and the cardinal direction (Figure 1). Each of these axes is associated with changes in gene expression and physiology or morphology, which we suggest are due in part to light and current direction and strength. It appears that polyps in the interior of

the colony are exposed to relatively stagnant conditions, whereas the colony periphery likely experiences higher flow, light exposure, chances for predation, and requirements for competition and defense leading to the dynamic physiological and transcriptional responses observed here. Our findings have implications for the interpretation of data from branches collected from different locations across multiple coral colonies. Specifically, when fragments are taken from multiple colonies for replication, considerations of the inherent differences across a colony should be included in sampling design. Our findings also shed new light on the potential drivers of plasticity of corals' responses to environmental stress and disease, and should be considered when reconstructing paleophysiology and past microenvironmental conditions from well preserved fossil coral colonies.

2 Manuscript Type

Original Research, Body text is 8048 words.

3 Methods

3.1 Field measurements

3.1.1 Sample collection

Ex situ measurements were conducted on a 15 cm diameter colony of *Stylophora pistillata* collected during the morning in April 2016 at 8 m depth under a special permit from the Israel Nature and Parks Authority in the coral nursery of the Inter-University Institute for Marine Science (IUI), Eilat, Israel using SCUBA (Figure 1a). The colony was brought to the lab in a tank filled with seawater and divided into individual branches and branch segments within 20 minutes of collection. Nine branches (numbered 1-9 in Figure 1b, c and supplementary materials) were taken from three horizontal concentric rings (one 'top' branch, four 'middle' branches, and four 'bottom' branches) and classified according to their relative height within the coral colony (Figure 1b, c). The eight middle and bottom branches also represent duplicates from each cardinal direction (N, S, E, W). All branches were further divided into sections according to their position on the branch (tip, junction, base) and flash-frozen in TRI-Reagent (Sigma) (Figure 1 inset) for differential gene expression analysis. Five additional branches (numbered 20-24 in Figure 1b, c and supplementary materials) distributed around the colony were chosen for physiological examination, fragmented into tip, junction, and base segments, and then kept at –80 ˚C.

3.1.2 Oxygen measurements

Immediately prior to removal of the colony intended for high spatial resolution examination from the coral nursery, dissolved oxygen (DO) in seawater between branches of five *S. pistillata* colonies located in the IUI coral nursery was measured in-situ. This nursery is a pair of raised 4x3 m frame structures (part of one can be seen behind the coral colony in Figure 1a) ranging in depth from 5-10 m, so that conditions experienced by all well-spaced colonies are quite similar across the nursery. Measurements were taken as up to five radial transects per colony, from inside to just outside each colony (i.e., center, mid-way, and periphery), using Unisense oxygen microsensors mounted on a Unisense UnderWater Meter System. The microsensors were moved through each colony at a controlled pace in order to keep the intra-colony water as undisturbed as possible and to prevent exchange of inter-branch water within the colony and with the surrounding water. Each measurement was taken for a duration of two minutes to allow the oxygen microsensor readings to stabilize. All measurements for each transect were normalized to

133 the outermost reading for that transect (Supplementary Table 1). DO concentrations across one
134 representative transect were calculated according to the following equation to establish that such
135 values were normoxic: DO (μmol/L) = (DO_{sat}(μmol/L)/(mV_{sat}-mV_0)) * in situ mV measurement.
136
137 *3.1.3 Microbial counts*
138 Microbial counts outside and within the coral colony were performed at the same time as DO
139 measurements on samples collected in-situ via radial transects on five different colonies growing
140 at the same site. We conducted preliminary experiments using small aliquots of concentrated
141 fluorescein dye injected to water between branches of *S. pistillata* skeletons, the same size as that
142 used in our physiological experiments, in a static laboratory aquarium to test the efficacy of
143 extracting water from between branches and at colony peripheries with minimal intra-colonial
144 water mixing. Briefly, we injected the dye on one side of a branch and then used a syringe to
145 carefully extract various volumes of water, from 0.4 to 12 ml in intervals of 0.4 ml, from the
146 other side of the branch, with five replicate experiments per extract volume tested. We then
147 measured the fluorescence of the extracted water, subtracted the fluorescence background of the
148 surrounding water, and represented the results as a percentage of the fluorescence from the
149 injected fluorescein dye aliquot. This showed that we could extract up to 1.6 ml of seawater from
150 between coral branches and from colony peripheries without pulling in water from the immediate
151 environment of the surrounding branches (Supplementary Figure 1). Water flow during our
152 sampling dive was noticeably very low. We therefore felt confident extracting 1 ml of seawater
153 from between the branches ('center' position) and the tip of the branch at the colony periphery
154 ('periphery' position).of the live colonies. Upon completion of the dive, all water samples were
155 immediately carried to the lab and fixed in cryovials in a final concentration of 0.0625%
156 glutaraldehyde, incubated in the dark for 10 minutes, and then flash-frozen at − 80 °C until
157 analysis by flow cytometry.
158
159 Just prior to analysis, microbial count samples were thawed at room temperature and diluted 1:1
160 in ultra-pure water, and 2 μm-diameter fluorescent beads were added to each sample as an
161 internal standard (Polysciences, Warminster, PA, USA). The samples were analyzed on a
162 FACSCanto™ II Flow Cytometry Analyzer Systems (BD Biosciences). We first examined the
163 natural fluorescence of the cells (chlorophyll and phycoerythrin pigments). We then stained the
164 cells with SYBR Green I (Molecular Probes/ThermoFisher) according to the manufacturer's
165 instructions and counted the total microbial population as well as cyanobacterial sub-populations.
166 Data were acquired and processed with FlowJo software. Flow rates of the instrument were
167 determined several times during each run and the average value for a sample-free test run was
168 used for calculating cell per ml.
169
170 **3.2 Physiological analysis**
171 *3.2.1 Tissue removal*
172 Tissue was removed from five frozen coral fragment skeleton by airbrush with phosphate
173 buffered saline (PBS) and homogenized using an electrical homogenizer (MRC, HOG-160-1/2)
174 for 10 seconds. A sub-sample of each fragment's homogenate was stored for cell counts,
175 chlorophyll extraction, and total protein measurements and the rest of the homogenate was
176 centrifuged for 5 minutes at 5000 rpm. The supernatant was retained for host protein and
177 hemolysis assay. The pellet was observed under the microscope to quantify photosynthetic

178 symbionts. All quantities were adjusted to fragment extraction volume and normalized to cm^2 of
179 the fragment's surface area.
180
181 *3.2.2 Chlorophyll extraction*
182 Two ml of tissue homogenate was filtered on a Whatman GF/C filter and incubated with 1 ml
183 90% acetone for two hours at 4°C. After incubation, the filter was manually homogenized and
184 the solution was filtered through a 0.22 µm syringe filter into a glass cuvette. Spectrophotometric
185 measurements were conducted on a NanoDrop (Thermo-Fisher) and chlorophyll a concentrations
186 were calculated from light absorbance results based on the following equation (Ritchie, 2008):
187 chl-a [mg/ml]= $-0.3319(ABS630)-1.7485(ABS_{647nm})+11.9442(ABS_{664nm})-1.4306(ABS_{691nm})$.
188
189 *3.2.3 Nematocysts and photosynthetic symbiont counts*
190 100 µl of tissue homogenate was used for nematocyst (supernatant) and photosymbiont (pellet)
191 counts by hemocytometer (BOECO, Germany); cells were counted in five randomly selected
192 fields per fragment (1 mm^2 each) on a Nikon Eclipse Ti-S Inverted Microscope System.
193 Nematocysts were counted under white light with a contrast filter whereas photosynthetic
194 symbionts were viewed by fluorescence at 440 nm excitation and 590 nm emission. NIS
195 ELEMENTS (Nikon) software was used for the cell counts with automatic counting settings
196 limited to cell diameters smaller than 15 µm and circularity set to >0.5 but <1.
197
198 *3.2.4 Total protein and host protein*
199 We quantified homogenate and host total protein; sonication (Ultrasonic Atomizer Probe
200 Sonicator) was used for further extraction of symbiont protein. Protein concentration of each
201 sample was measured by bicinchoninic acid (BCA) assay (Pierce) against a bovine serum
202 albumin standard curve at an absorbance of 540 nm.
203
204 *3.2.4 Hemolysis assay*
205 Hemolytic assays were performed against O Rh positive human blood cells obtained from the
206 Rambam/Yoseftal Hospital Blood Bank, as described previously (Primor and Zlotkin, 1975).
207 Briefly, 2 ml of whole blood was diluted to a final volume of 15 ml in PBS (pH 7.4) and
208 centrifuged at 3000 g for 5 min. The supernatant was removed, and the process was repeated
209 with the pelleted erythrocytes until the supernatant was clear. Washed erythrocytes were then
210 resuspended in PBS to a final concentration of 20% (v/v). For each hemolysis assay, 160 µl of
211 homogenate supernatant was incubated with 40 µl of washed erythrocyte suspension (4%
212 erythrocytes v/v) at 37°C for 30 minutes in a water bath. At the end of the incubation, 400 µl of
213 PBS was added, and the assays were centrifuged at 3000 g for 3 min. The supernatant fluid
214 containing the hemoglobin released from lysed erythrocytes was transferred to 96-well
215 microplates and the absorbance at 540 nm was determined on a spectrophotometric microplate
216 reader (Perkin-Elmer). In addition, each experiment was normalized to a positive (100%
217 hemolysis) and negative control (0% hemolysis) by incubating erythrocytes with DDW and PBS
218 alone, respectively. HU_{50} was defined as the amount of homogenate required to cause 50%
219 hemolysis (Bartosz et al., 2008) in a dilution series of the coral extract.
220
221 *3.2.5 Fragment surface area*
222 Surface areas were estimated using the aluminum foil method (Marsh Jr, 1970). Briefly,
223 aluminum foil was molded over the skeleton of each fragment (without measuring skeleton

connective areas between the divided fragments), carefully removed, and weighed. This was repeated three times on every fragment and the surface area was estimated using a standard curve of the derived relationship between foil area and weight.

3.2.6 Skeleton cleaning for assessments of surface area and corallite measurements

After tissue extraction, all fragments were cleaned of organic residues overnight in 3% sodium hypochlorite; the skeletons were then washed in deionized water and dried at 55°C.

3.2.7 Micromorphological analysis

The distance between neighboring polyps and the surface area of the polyp was measured using a Nikon binocular microscope and analyzed using NIS-Elements (Nikon) software. For each coral fragment, at least four corallites located in a position parallel to the focal plane were chosen. Major and minor axes and circularity were measured for each corallite and the ratio of the two axes (major divided by minor) was calculated; a ratio of 1 indicates a circle and the larger the ratio, the more elliptical the shape. Surface area of each measured corallite was calculated from the two-measured axes, using the following equation: $S = \pi * r$ (major axes)* r (minor axes). Finally, distances between neighboring corallites were also measured to evaluate polyp density in each area. Corallites were qualitatively analyzed by scanning electron microscopy.

3.3 Differential Gene Expression Analysis

3.3.1 RNA extraction, processing, and sequencing

Nine branches, each segmented into three portions along their axes, yielded 36 transcriptome libraries across the three-dimensional space of the coral colony (Figure 1, colony locations in Supplementary Table 3, read count statistics in Supplementary Table 4). Total RNA was extracted from the holobiont in fragments stored in TRI-Reagent (Sigma) following the manufacturer's protocol, with some modification at the homogenization step. Briefly, samples frozen in TRI-Reagent were heated and centrifuged, and then bromochloropropane, at a ratio of 1:10, was added to the samples for separation. After incubation at room temperature for 10 minutes and centrifugation, RNA was purified from the clear phase using a Purelink RNA Mini Kit (Ambion) according to the manufacturer's protocol. The RNA was washed in 70% ethanol and then on-column DNase digestion was performed using a Qiagen RNase-free DNase Kit according to the manufacturer's protocol. RNA-Seq libraries were prepared using an in-house protocol at the Weizmann Institute of Science. Briefly, the polyA fraction (mRNA) was purified from 500 ng of total RNA per sample followed by fragmentation and generation of double-stranded cDNA. Then, end repair, A base addition, adapter ligation and PCR amplification steps were performed. Libraries were evaluated by Qubit (Thermo Fisher) and TapeStation (Agilent). Sequencing libraries were constructed with barcodes to allow multiplexing of all samples to be run in each lane. Approximately 578 million total high-quality 125 bp paired end reads (15.45 ± 1.5 million paired reads per sample) were sequenced on an Illumina HiSeq 2500 across three different lanes (i.e., each sample run in triplicate to remove batch effects).

3.3.2 Host and symbiont RNA-Seq differential expression analysis

Standard RNA-Seq quality filtering was conducted as described previously (Malik et al., 2021). Briefly, RNA-Seq reads were adapter-trimmed using cutadapt 1.15 (https://cutadapt.readthedocs.io), and then low-quality regions were removed with Trimmomatic 0.3 (Love et al., 2014). In order to detect correct taxonomic classifications within our

transcriptome data, high-quality reads were mapped to all available NCBI and Reefgenomics (reefgenomics.org; (Liew et al., 2016)) genome-based proteome databases of Symbiodiniaceae species *Symbiodinium microadraticum, Cladocopium goreaui*, and *Fugacium kawagutii* (formerly *Symbiodinium* spp. clades A, C1, and F, respectively (LaJeunesse et al., 2018)), and Cnidaria as well as selected stramenopiles/alveolates/Rhizaria and Metazoa databases using Diamond (Buchfink et al., 2015). Top hits almost exclusively belonged to robust corals (mainly *S. pistillata*), and *S. microadriaticum* (formerly "clade A" (LaJeunesse et al., 2018)). These results are expected since *S. microadriaticum* was found to be a predominant symbiont in shallow water in Eilat (Malik et al., 2021). For symbiont RNA-Seq mapping, we further aligned the reads to the merged host genome assembly (NCBI GCA_002571385.1) and the symbiont genome assembly (NCBI GCA_001939145.1) using STAR (Dobin et al., 2013;Aranda et al., 2016;Voolstra et al., 2017). Across all branch fragments, 72-80% (~11-16 million reads) were concordantly mapped to the host genome, and 2%-10% (~0.5-1.5 million reads) were concordantly mapped to the symbiont genome. In total, 83-84% of the reads were aligned to either host or symbiont genomes. Differential expression (DE) analysis was conducted using Bioconductor DEseq2 (Love et al., 2014), separately for the host and the symbiont genes, using a DEseq2 generalized linear model. Specifically, we tested: (1) the additive effect of branch position, ring height and cardinal direction; (2) the additive and interaction effect of branch position and ring height (excluding cardinal direction factor); (Supplementary Tables 5-7). Note that the first model cannot include the four top branch samples (two tips, junction, base), since the single top branch is represented by an incomparable cardinal direction ("center"); as such, these samples were excluded from the analysis of expression of putative toxins and known biomineralization-related genes. For the symbiont analysis, only the first model was used. Although DESeq2 is designed to analyze samples of variable total read counts, in order to avoid read normalization problems, we only selected symbiont genes whose 25% quantile of read count was at least 12 reads (with 12,735 symbiont genes remaining); further, only symbiont samples with >300k total reads were retained. After filtering, the correct symbiont read normalization was indicated by a typical close-to-symmetric distribution of fold-changes around the DESeq2 MA plot horizontal axis (Supplementary Figure 2). NMDS analysis was conducted using metaDMS in the R Vegan package based on $\log_{10}$FPM values of all expressed genes. For the symbiont NMDS, since read counts were relatively low, pairs of tips from the same branch are represented together based on the sum of read counts for both tips; however, symbiont DESeq2 data were not pooled for differential gene expression analysis.

3.3.3 Branch genetics and SNPs analysis

Single nucleotide polymorphisms (SNPs) analysis was conducted for each sample using the Broad Institute-recommended RNA-Seq SNPs practice (https://gatk.broadinstitute.org). The pipeline includes four steps: STAR reads mapping, a pre-processing step aimed at removing various alignment biases, variant calling using GATK version 3.5, and finally variant filtration and annotation (DePristo et al., 2011). In order to exclude variant-call biases due to changes in transcript abundance between samples, we considered only SNP loci with coverage greater than 30 RNA-Seq reads in all tested samples. Identity By Decent (IBD) analysis was conducted using SNPRealte in R.

3.3.4 Host and symbiont functional enrichment analysis

Biological terms were assigned to genes based on Uniprot *S. pistillata* (www.uniprot.org), KEGG *S. pistillata* (www.kegg.jp), *S. pistillata* Trinotate annotations (Bryant et al., 2017), and Uniprot *S. microadriaticum* databases. Enrichment analysis was conducted in Bioconductor GOSeq (Young et al., 2012), which corrects for enrichment biases associated with correlations between gene size and DE significance. We also searched for functional enrichment using the score-based tool GSEA (Subramanian et al., 2005;Sergushichev, 2016), which may be more sensitive than p-value cutoff-based searches (such as GOSeq) when small non-significant changes in relatively large groups of genes are expected. In GSEA, we used $\log_2$ fold changes as scores. Because many enriched terms are functionally related, we hierarchically clustered the biological terms based on pairwise distances between groups of genes: $D = |xa \cap xb| / \text{minimum}(|a|,|b|)$, where a,b are two sets of gene ids, and xa and xa are DE genes ids from a and b, respectively. Terms trees were constructed using Bioconductor-ggtree (Yu et al., 2018). Terms enriched in ring height comparisons to the top of the colony should be viewed with caution as only one branch was taken from that classification. Only significant enrichment results are reported.

3.3.5 Focused S. pistillata *gene analyses*

Putative toxin genes were identified using reciprocal best-BLAST hits as described in (Rachamim et al., 2015;Yosef et al., 2020) (Supplementary Table 14).Differential expression of genes coding for known biomineralization-related proteins from *S. pistillata* skeleton or the calicoblastic layer were examined (Puverel et al., 2005;Drake et al., 2013;Mass et al., 2013;Zoccola et al., 2015;Peled et al., 2020) (Supplementary Table 16).

3.4 Statistical Analyses

Statistical tests of all skeletal, physiological, and environmental data described above were performed in RStudio (RStudio Team). If a parameter displayed both homogeneity of variance (Fligner-Killeen test) and normal distribution (Shapiro-Wilke test), a one-way ANOVA (chlorophyll/total protein, chlorophyll/photosymbiont cell, photosymbiont/surface area, total protein/surface area, host protein/surface area, nematocysts/total protein, nematocysts/surface area, corallite diameter, corallite distanc) was performed, with TukeyHSD post hoc analysis for parameters with significant differences between locations. Parameters with non-homogenous variance and/or non-normal distribution were analyzed using Wilcoxon's rank sum test (water column microbes, DO) or the Kruskal-Wallis rank sum test (chlorophyll/surface area, photosymbiont/total protein, hemolytic units/total protein, hemolytic units/surface area, corallite axis ratio), with Dunn's test for post hoc analysis for parameters with significant differences between locations. Environmental parameters were pooled between all colonies and tested between measured locations as described above. Coral and photosymbiont physiological and morphological parameters were tested between branch axis locations across the colony (i.e., five replicates each of junctions and bases, and 10 replicates of tips); however, there was not sufficient replication at cardinal directions or ring height for statistical evaluation of parameters between these locational classifications.

4 Results and Discussion

4.1 Differences in water DO and microbial counts across colony structure

Because branching corals' three-dimensional structure can lead to different micro-environments within the colony, we first aimed to characterize indicators of the environmental conditions

experienced by polyps at different locations within the colony that could potentially affect their gene expression. Rather than making direct measurements of flow within *S. pistillata* colonies at the IUI reef, we instead measured several within-colony water parameters affected by flow. We focused on dissolved oxygen because its concentration can vary within coral colonies, affecting coral physiology (e.g., Mass et al., 2010). Likewise, microbial counts represent an easy to quantify variable that can be used as a proxy of water stability. We measured higher oxygen concentrations in water collected close to the core (center; ~250 μmol/L) of the corals, compared to samples collected at colony peripheries (~230 μmol/L; $p<0.05$, Wilcoxon rank sum test; Figure 2a; Supplementary Tables 1, 2). Although there was variability in DO signal between colonies (Supplementary Figure 3), the 'center' versus 'periphery' differences held across all colonies. We also observed higher microbe densities in water collected from the colony interiors versus the immediately surrounding seawater ($p<0.05$, Wilcoxon rank sum test; Figure 2b; Supplementary Tables 1, 2). Both of these observations may be due to lower rates of water exchange at branch bases due to decreased water flow within the colony, as suggested by (Chang et al., 2009). Lower mass transport has been observed within the less densely branched *Pocillopora eydouxi* whose overall colony structure is similar to the *S. pistillata* studied here (Figure 1a) compared to the more densely branched *P. meandrina* (Hossain and Staples). Flow reduction within the colony would cause the accumulation of oxygen produced by photosynthesis (Mass et al.) and we speculate might also support the retention of microbes actively growing between branches (e.g., Schiller and Herndl;Ritchie, 2006), or those chemotaxing toward the coral tissue (Garren et al., 2014). These differences further support the notion that the environment differs along the coral branches from colony exterior to interior and may affect the coral holobiont with some polyps inhabiting more or less favorable areas, which we observe being reflected in transcriptomic and physiological differences across the colony.

4.2 Location-specific intracolonial variability of physiology and gene expression

To assess how the differences in environmental conditions resulted in different physiology and gene expression across a colony, immediately after measuring DO and collecting microbial samples we removed a single *S. pistillata* colony from the IUI reef, We then examined its branches both at different cardinal directions and heights above the substrate (i.e., ring height), with each branch further segmented along its axis from base to tip (Figure 1 inset; Supplementary Table 3). The identified patterns in gene expression and physiology therefore represent responses to microenvironments experienced by the colony at the specific time of collection and depth at which the colony was growing. The *S. pistillata* colony examined here was genetically homogenous (not chimeric, Supplementary Figure 4), and thus any changes in physiology or gene expression between regions were likely a response of the polyps to their local micro-environmental conditions rather than genotypic differences. While our study was limited to a single colony to achieve high spatial resolution of data, many similar genetic patterns are conserved between two major stony coral clades (see below). Additionally, differences were observed in hemolytic potential between branch tips and bases, which were seen also in two additional colonies from an independent study (Ben-Ari et al.). Taken together, it is clear that there are transcriptional and physiological differences between various locations within the coral colony, and that many of these differences are likely to be common across branching colonial corals. The expression of >10,000 of the ~24,000 tested host genes was affected by at least one of the tested factors: location at branch, ring height, and cardinal direction (Supplementary Tables 4-6). We observed a clear differentiation in host gene expression between branch

407 positions and from the top to the bottom of the colony (Figure 2c, Figure 3, Supplementary Table
408 5), although comparisons to the lone top branch should be viewed with caution. Combined, we
409 observed an interaction effect between factors (Supplementary Tables 4, 6), as, for instance,
410 groups of genes involved in signaling pathways important in development that were significantly
411 enriched in branch tips versus bases as compared to middle versus bottom interactions (Figure
412 3b, Supplementary Figure 5). Comparing colony interior with periphery, host gene expression
413 patterns are more similar between junction and base branch positions compared to tips, although
414 not the same at junctions and bases (Figure 2c). In contrast to the roughly ½ of all tested genes
415 showing differential expression between location classifications, the only physiological
416 parameters that differed along branch axis were hemolytic potential and skeleton morphology
417 (described in detail below). Elucidating the microenvironmental drivers of these genetic and
418 physiological differences across a colony may aid in, for example, understanding spatial
419 differences of polyps' interactions with various infectious organisms that target the oral ectoderm
420 (e.g., Gibbin et al.) leading to diseases such as skeletal band eroding disease (Winkler et al.,
421 2004), which has been observed to commence at colony interiors. Other previously reported
422 response differences across colonies that may be due to microenvironmental variations include
423 bleaching that commences at colony perimeters in *Oculina* (Shenkar et al., 2005), greater storage
424 of lipids and total fatty acids toward colony interiors in *Acropora* (Conlan et al., 2018), and
425 differing relative abundance of various photosymbiont species in regions that later displayed
426 differential bleaching susceptibility (Kemp et al., 2014).
427
428 In contrast to the host, of ~12,000 tested photosymbiont genes, only ~150 were differentially
429 expressed (DE) (Supplementary Table 7). The host vs. symbiont differences are partly attributed
430 to technical differences in statistical power due to lower symbiont read counts, and likely
431 represent an underestimation of symbiont DE genes. DE gene patterns of the photosymbionts are
432 not as clearly delineated as for the host (Figure 2d); nevertheless, the expression patterns differ
433 between cardinal directions ($p<0.0007$, ADONIS test, Supplementary Table 8), likely reflecting
434 the different light regimes experienced on different sides of the colony, visible as shading on the
435 north (right) side of the colony and no shading on the south (left) side of the colony in Figure 1a,
436 although we did not measure light levels around the colony. The ultimate drivers of the
437 differences observed for groups of polyps in locations differing by ring height and cardinal
438 direction remain to be resolved. Further, the observed differences across a single colony could
439 have implications for studies using branches collected from different locations on separate
440 colonies. While intracolonial differences that may diminish observable transcriptional and
441 physiological differences between treatments - if chosen branches are from differing parts of
442 selected colonies - may lessen over multi-year studies (e.g., Palumbi et al., 2014), epigenetic
443 responses that differ across a colony may persist across generations (Liew et al., 2020).
444
445 *4.3 Patterns in gene expression are conserved between coral taxa*
446 A previous study, analyzing the differences in gene expression between branch tips and bases in
447 *Acropora* spp. (Hemond et al., 2014), provided an opportunity to identify conserved intra-
448 colonial patterns in gene expression between these two coral taxa, which likely diverged at least
449 200 million years ago (Park et al., 2012). We identified ~9,600 putative orthologous expressed
450 genes between *S. pistillata* and two species of *Acropora* spp. (Hemond et al., 2014), based on
451 reciprocal BLAST. Interestingly, from a total of 952 genes that were DE in *Acropora* spp. along
452 the branch axis, ~70% were also DE in *S. pistillata* (672), and ~90% of these exhibited the same

453 fold change trend (p-value < 2.2e-16, Fisher's exact test; Figure 3a, Supplementary Table 9).
454 Overall, these results indicate that micro-environmental dependence of gene differential
455 expression at tips versus bases reflects an evolutionarily conserved pattern rather than a species-
456 specific pattern, being observed in members of both robust (here) and complex (Hemond et al.,
457 2014) scleractinian clades, as well as between taxa which possess physiologically unique axial
458 polyps (*Acropora*; (Wallace, 1978;1985) and a genus which does not (*Stylophora*). It also
459 supports that the occurrence of intracolonial differential responses to microenvironments in
460 general, and up-regulation of genes for specific processes such as protein production and energy
461 generation in particular (Figure 3b, green font), can likely be generalized across branching coral
462 taxa.
463
464 *4.4 Gene expression patterns suggest differences in host versus photosymbiont metabolism*
465 We next inferred potential broad-scale changes in cellular and metabolic functions by identifying
466 KEGG and Gene Ontology (GO) enrichment patterns associated with micro-environmental
467 changes in both the host (Figure 3b, Supplementary Tables 10, 11) and the photosymbiont
468 (Figure 3c, Supplementary Table 12). As expected, broad clusters of host KEGG terms and
469 photosymbiont GO terms were DE (Figure 3b, c), mirroring the pattern observed for all DE
470 genes within the host and symbiont (Figure 2c, d), with many more terms DE in the coral host
471 along the branch axis compared to the ring height or cardinal direction (Figure 3b), and more
472 terms differed along cardinal direction for the photosymbiont (Figure 3c).
473
474 Most DE host genes grouped by KEGG term tended to be up-regulated in branch tips relative to
475 the junctions or bases (Figure 3b, Supplementary Tables 10, 11). Specifically, many terms
476 related to cell metabolism were enriched in the tips versus the bases, including carbohydrate
477 metabolism (e.g., glycolysis and the TCA cycle, oxidative phosphorylation, mitochondrial
478 biosynthesis), amino acid biosynthesis and metabolism, and lipid metabolism (Figure 3b). We
479 further tested which functional groups were enriched with conserved tip vs. base DE gene
480 patterns between coral taxa (Figure 3a, b). As indicated by green KEGG term text in Figure 3b,
481 many fundamental processes such as metabolism show similar DE trends and enrichment
482 between these two genera (Supplementary Tables 9, 10), indicating a conserved response
483 between the taxa. "Zooming in" from the KEGG terms to the underlying genes, we note that
484 genes related to oxidative phosphorylation, such as ATP synthase, cytochrome c oxidase, co-
485 enzyme Q, and NADH dehydrogenase tend to be up-regulated at branch tips across the species.
486 In addition, multiple genes for succinate dehydrogenase as well as other individual genes
487 comprising the citric acid cycle, were also more highly expressed at branch tips than junctions or
488 bases in *S. pistillata* and many of these showed similar regulation patterns in the *Acropora* spp.
489 Finally, most of the >100 DE genes with KEGG terms for mitochondrial biogenesis were up-
490 regulated at tips compared with junctions and bases in *S. pistillata* and many of their likely
491 homologs were also up-regulated at branch tips in *Acropora* spp. The increased rates in
492 physiological processes involved in energy production at branch tips, as suggested by our gene
493 expression analysis, have been observed in the branching coral *A. palmata* as increased
494 respiration and mitotic index (Gladfelter et al., 1989).
495
496 Intriguingly, the patterns of gene expression observed in the host were not all recapitulated in the
497 photosymbiont. Although some symbiont GO terms associated with photosynthesis were
498 enriched in the tips vs bases in the symbionts (e.g., those involved in light-harvesting and the

499 thylakoid), likely in response to higher light intensities at tips compared to bases (e.g., Helmuth
500 et al., 1997;Kaniewska et al., 2008), others were not, including terms involved with carbon
501 fixation (Figure 3c). Additionally, no differing patterns in photophysiology were found along
502 branch axis, measured here as chlorophyll and symbiont density per both total protein and area
503 (Supplementary Tables 2, 13, Supplementary Figure 6), although we acknowledge that these are
504 limited measures of the photophysiological processes. Indeed, previous studies have shown that
505 the products of photosynthesis can be translocated from branch bases to the tips in branching
506 corals (e.g., Rinkevich and Loya). Rather than exhibiting tip-to-base functional differences,
507 many of the terms associated with symbiont photosynthesis (both light and dark reactions) were
508 found to differ along cardinal direction, being enriched in south-facing branches (Figure 3c),
509 possibly due to the direction of the sun. As such, we anticipate that future studies will find
510 differences in gene expression in the symbiont across a diel cycle, with, for example potentially
511 decreased differences between north- and south-facing branches during nighttime hours. As
512 noted above, these enrichment patterns are likely an underestimation. Furthermore, correlations
513 between mRNA abundance and physiological patterns may not be high due to translation level
514 effects, translocation of host/symbiont products, food particle capture by the host, etc., which
515 may lead to differences in symbiont transcriptional control.
516
517 *4.5 Developmental pathways are DE along the branch axis*
518 In addition to pathways related to metabolism, several KEGG terms associated with development
519 and morphological plasticity in colony architecture were DE between branch tips and junctions
520 or bases. For example, the Wnt signaling pathway was enriched at branch tips versus the bases in
521 both *S. pistillata* (Figure 3b) and *Acropora* spp. (Hemond et al., 2014). This pathway, which
522 transmits information from outside to inside cells, is associated with cell differentiation and axis
523 patterning in cnidarians (reviewed in Lee et al., 2006;e.g., Duffy et al., 2010) and bilaterians
524 (e.g., Siegfried and Perrimon). Similarly, the TGFβ signaling pathway was also enriched in *S.*
525 *pistillata* branch tips (Figure 3b), although this was not observed in *Acropora* spp. (Hemond et
526 al., 2014); this pathway has been implicated for a role in development and calcification in corals
527 (Gutner-Hoch et al., 2017). At the individual gene level, we observed that fibroblast growth
528 factors, which could aid in development of limbs (reviewed in Xu et al., 1999) and in production
529 of nerve cells (reviewed in Guillemot and Zimmer, 2011), were significantly up-regulated at
530 branch tips. Half of the genes involved in mitochondrial biosynthesis were also up-regulated at
531 branch tips. Further, two different bone morphogenetic proteins (BMPs), which may play a role
532 in axial patterning in cnidarian polyps (Reinhardt et al., 2004) and in budding (Surekha et al.,
533 2020), were up-regulated at branch tips here. Finally, several retinol dehydrogenases, proteins
534 associated with photoreceptors in higher organisms (Albalat, 2012), were up-regulated at branch
535 tips, where light levels tend to be higher, an observation shared with *Acropora* spp. (Hemond et
536 al., 2014).
537
538 In addition to the plasticity described above, gamete production has also been shown to vary
539 along branches axes across several coral taxa with gametogenesis typically occurring
540 preferentially deeper in the colony (e.g., Stimson). We observed the highest expression of several
541 testis-specific genes, such as testis-specific chromodomain protein Y 1-like and testis-specific
542 protein kinases at *S. pistillata* branch junctions (Supplementary Table 4). In humans, these genes
543 are associated with chromosome Y (Lahn and Page) and/or may be involved in sperm structure
544 (Walden and Cowan). Interestingly, we observed up-regulation of octopamine receptors at

545 branch tips, suggestive of higher maturation of ovaries and testes in that location (Chiu et al.,
546 2020).
547
548 *4.6 Changes in expression of genes potentially related to predation along branch axis*
549 As described above, many metabolic processes were enriched in the tips versus the bases,
550 whereas there is little evidence for higher photosynthesis by photosymbionts at branch tips.
551 Asking whether this could be due to more heterotrophic food input in the tips (e.g., through
552 predation), we analyzed the tissue toxicity (hemolytic activity) and gene expression patterns of
553 putative toxins. Although there was no difference in nematocyst abundance along branch axes
554 (Figure 4a, Supplementary Table 2), tissue hemolytic activity was highest at branch tips (Figure
555 4b, Supplementary Table 2), consistent with previous studies in *S. pistillata* that used branches
556 from two different colonies (Ben-Ari et al.). Thus, the observed branch axis patterning of
557 hemolysis potential is robust across at least three colonies from two independent studies. Using
558 reciprocal BLAST, we identified 22 putative toxin genes (Rachamim et al., 2015), encoding
559 cytolysins, phospholipase A2 toxins, SCRiPs (small cysteine rich peptides) and a potential
560 Kunitz/K channel toxin (Supplementary Table 14). We also compared these genes to the
561 reciprocal BLAST results against the *Acropora* spp. dataset (Hemond et al., 2014), finding only
562 two orthologous matches, a SCRiP and an uncharacterized protein. Like their *S. pistillata*
563 counterparts, they were not DE between branch tips and bases (Supplementary Table 15). In our
564 putative toxin dataset, we observed 13 and 11 DE genes between branch tips versus bases or
565 junctions, respectively (Figure 4c, d; Supplementary Table 15, Supplementary Figure 7). Up-
566 regulation of genes encoding potential toxins at branch tips has previously been observed in
567 colonial corals (Hemond et al.;Hemond and Vollmer). The two most abundantly expressed
568 putative toxin genes encode for a cytolysin (up-regulated at tips) and a second SCRiP (up-
569 regulated at bases), with the rest of the toxin genes having much lower overall expression levels
570 (Figure 4c, d; Supplementary Table 15). The highly expressed cytolysin is of particular interest
571 as it belongs to the actinoporin family, and a hemolytic protein from this family, likely the
572 protein or an isoform of the highly expressed gene here (Supplementary Figure 8), has
573 previously been isolated from *S. pistillata* (Ben-Ari et al., 2018). Actinoporins are ~20 kDa
574 water-soluble proteins which are lethal when injected into crustaceans (Giese et al., 1996), and
575 which insert themselves into membranes, particularly those containing sphingomyelins (Alvarez
576 et al., 2009). They have been immunolocalized to tentacle nematocysts as well as to mesenterial
577 filaments (Basulto et al., 2006). SCRiPs are ~5 kDa peptides which may be anthozoan-specific
578 (Sunagawa et al.;Jouiaei et al., 2015), with evidence that they have neurotoxic effects (Jouiaei et
579 al., 2015), although their function remains to be fully clarified.
580
581 The higher hemolytic activity and larger number of toxins more abundantly expressed at branch
582 tips suggest that the tips play the dominant role in venom-based competition, defense, and
583 predation, although more work is needed to identify the role of putative toxins such as SCRiPs,
584 which were more abundantly expressed at branch bases, and the potential contribution and roles
585 of photosymbiont toxin production (e.g., Nakamura et al., 1993). While it is difficult to
586 disentangle toxin effects on competition and defense from predation, based on higher flow at the
587 edges of colonies (Chang et al., 2009), colonies' edges are likely exposed to higher food loads
588 than are areas closer to the base of the branches. Consumption of these food sources could then
589 be reflected in increased respiration rates as the food is metabolized, as has been observed in
590 other species (Gladfelter et al., 1989) and may yield increased energy production which would

591 require up-regulation of genes involved in this process as we observed here. We also queried
592 genes related to digestion and observed that many peptidases were DE, but not in a clear pattern
593 along the branches with approximately half up-regulated at the tips. Similarly, multiple lipases
594 were DE between branch locations, but no general trend was observed. However, pancreatic
595 lipase expression, which has been observed in gastric cirri in a scyphozoan (Steinmetz, 2019),
596 was found to be significantly up-regulated to a high degree at branch tips. We also observed up-
597 regulation of three chitinases in branch tips versus bases, which could support extracellular
598 digestion of arthropod prey (Steinmetz, 2019). In contrast, an amylase which converts starch and
599 glycogen - biomolecules used by the photosymbiont and host, respectively, to store
600 photosynthates (Kopp et al., 2015) - into simple sugars, was down-regulated at the tips versus
601 junctions and bases. Thus, while our results suggest differences along the branch axis of
602 functions related to prey capture and defense, including both toxicity and digestion, further work
603 is needed to fully characterize the relative contributions of photosynthesized products and
604 predation. Additionally, temporal differences in predation capabilities at both the transcriptional
605 (i.e., genes related to digestion) and physiological (i.e., hemolytic potential) levels across
606 individual colonies should be examined as zooplankton abundance on coral reefs changes on a
607 diel cycle (Yahel et al., 2005). Future studies measuring water flow rates explicitly in
608 conjunction with transcriptional changes across colonies with complex macromorphologies will
609 also clarify precisely how particle capture and digestion are affected by differing flow patterns
610 (e.g., Sebens et al., 1997).
611
612 *4.7 Changes in skeleton structure and expression of known biomineralization genes along*
613 *branch axis*
614 Shallow water stony corals are most notable for their production of massive reef structures,
615 growing in size by adding mineral and new polyps, particularly for branching corals, at colony
616 tips or edges (e.g., D'A and Le Tissier, 1988;Meesters and Bak, 1995). We therefore examined in
617 depth skeletal morphological patterns and related gene expression across the three branch axis
618 locations. Unlike most other physiological parameters across the colony which were not
619 significantly different between branch positions (Supplementary Tables 2, 13), those linked to
620 differences in biomineralization were significantly different along branch axes. Qualitatively,
621 coenosteal spines appear narrowest and thinnest at the tip while base spines exhibit a more
622 distinct microtuberculate texture in their lower portions (Figure 5aii, iv, and vi). Such
623 microtuberculate texture with better differentiation of mineral fiber bundles may suggest higher
624 organic matrix content which separates the mineral phase packages to a greater extent (Mass et
625 al., 2014;Coronado et al., 2019). Corallites were closer together and more elliptically shaped at
626 the tips than at the branch junctions or bases (Figure 5b and c; Supplementary Tables 2, 13).
627 Comparable trending toward ellipticity at branch tips has been reported in other Pocilloporids
628 (Schmidt-Roach et al., 2014). Further, genetically identical *S. pistillata* branches have been
629 shown to have more distantly spaced corallites with thicker theca and longer septa when grown
630 under light spectra biased toward blue wavelengths (Rocha et al., 2014). While we did not
631 measure light spectra in this study, such a spectral shift along a single branch, due to absorbance
632 of red light by water, has been observed in *S. pistillata* tissue at the colony level on the sides
633 versus at the top of ~30 cm diameter colonies (Kaniewska et al., 2011) and at the branch level
634 along *Acropora millepora* branches toward the colony interior (Wangpraseurt et al., 2014).
635

636 We next examined differential expression of genes encoding proteins sequenced from *S.*
637 *pistillata* skeleton and likely directly involved in the calcification mechanism (Puverel et al.,
638 2005;Bertucci et al., 2011;Drake et al., 2013;Mass et al., 2014;Peled et al., 2020;Mummadisetti
639 et al., 2021), as well as a bicarbonate anion transporter observed predominantly in the
640 calicoblastic cell layer (Zoccola et al., 2015) (Figure 5e; Supplementary Table 16,
641 Supplementary Figure 9). We did not include genes for known skeletal proteins from *Acropora*
642 *millepora* and *A. digitifera* (Ramos-Silva et al.;Takeuchi et al.), as not all orthologs have been
643 found in *S. pistillata* skeleton although they exist in the genome, or non-orthologous proteins
644 within the same functional group occur in *S. pistillata* skeleton (Zaquin et al., 2021). Similar to
645 the global gene expression pattern for the host, we observed an up-regulation of
646 biomineralization genes biased toward the tips (Figure 5d, e; Supplementary Table 16). Of the 36
647 biomineralization-related genes that were DE between branch tips and bases, eight orthologous
648 genes were also DE and in the same direction in *Acropora* spp. (Hemond et al., 2014)
649 (Supplementary Table 17). In *S. pistillata*, the bicarbonate anion transporter SLCγ4, a coadhesin-
650 like protein, uncharacterized skeletal organic matrix protein 8 (USOMP8), and a hypothetical
651 protein were up-regulated at branch tips but were expressed in only low amounts. In contrast, a
652 ZP-domain containing protein, carbonic anhydrase (STPCA2), mammalian ependymin-related
653 protein, and coral acid rich protein 3 (CARP3) were moderately up-regulated at branch tips and
654 were very highly expressed overall. These proteins exhibit very different functions with SLCγ4
655 and STPCA2 involved in regulating carbonate chemistry within the calcifying space (Zoccola et
656 al., 2015;Zoccola et al., 2016), while CARP3, which is a highly acidic protein (35% Asp,
657 15%Glu (Mass et al., 2013)) can direct mineralogy toward formation of Mg-calcite and vaterite
658 (Gavriel et al., 2018;Laipnik et al., 2020), and is up-regulated in newly-settled coral polyps
659 (Akiva et al., 2018), in colonies growing at shallow depths (Malik et al., 2021), and in coral cell
660 cultures reared at increased pCO_2 (Drake et al., 2017). Although the function of USOMP8 is not
661 known, it is structurally similar to a BMP inhibitor (Drake et al., 2013). Of the remaining known
662 highly acidic coral skeleton genes, CARPs 1 and 4 (CARP4 is sometimes also called skeletal
663 aspartic acid rich protein 1; SAARP1 (Ramos-Silva et al., 2013)) were up-regulated at branch
664 tips and were moderately expressed; both proteins are biased toward Asp residues (Mass et al.,
665 2013) and are likely involved in nucleation initiation in early mineralization zones of growing
666 septa (Mass et al., 2014). In contrast, CARP2 exhibited very low although significantly up-
667 regulated expression at branch tips; while this protein is suggested to have a role in skeleton
668 extension based on its localization to more soluble growth areas (Mass et al., 2014), its down-
669 regulation upon settlement in pocilloporid larvae (Mass et al., 2016;Akiva et al., 2018),
670 association with ACC phases pre-settlement (Akiva et al., 2018), and low overall expression in
671 the present study may instead point to a role in inhibiting aragonite nucleation.
672
673 Previous and our present work provide strong genetic support for highest biomineralization
674 activity at branch tips (e.g., Goreau, 1959). This faster calcification at the tips may result in the
675 qualitatively thinner and narrower coenosteal spines we observed at branch tips (Figure 5) that
676 would be thickened by polyps as they age. Energy for higher calcification rates at branch tips
677 could come from two sources. First, there is evidence of translocation of ATP from tissue
678 regions deeper in the colony with relatively high photosynthetic rates (Fang et al., 1989) to
679 branch tips. Secondly, our and previous data suggest that the potential for predation is higher at
680 branch tips, with higher toxin gene expression and hemolytic activity at that location (Figure 4)
681 (Hemond et al., 2014;Ben-Ari et al., 2018), and up-regulation of genes related to metabolism and

energy production (Figure 3). This further suggests that biomineralization gene expression and skeleton morphology patterns observed at the sub-polyp scale (i.e., centers of calcification in growing tips of septa) are recapitulated at the branch scale (Malik et al., 2021).

5 Summary and Conclusions

Some colonial cnidarians, particularly hydrozoans, exhibit a clear division of labor inside the colony, with functionally and morphologically distinct polyps across the colony (Cartwright et al., 1999). While no obvious division of labor at the polyp scale is observed in corals, our results show, from molecular to physiological and morphological scales on a single genetically-identical colony, a functional specialization by clusters of polyps due to their locations on coral branches and around the colony likely related to the microenvironments they encounter (Rueffler et al., 2012) (Figure 6). In simplest terms, polyps at branch tips and toward the top of the colony are more exposed to light and higher water flow than are those found lower in the branches and closer to the substrate with consequent differential expression of a multitude of genes directing many key functions and, at least along the branch axis, differences in physiology and skeleton morphology. Our findings suggest that branch tips may also be sites of higher potential for envenomation for colony defense and predation, as well as possibly for enhanced prey capture. These plastic responses by genetically identical polyps can then be communicated through the coenosarc to the rest of the colony to allow for enhanced resource sharing (Mackie, 1986). Such plasticity may aid in colony recovery after partial mortality events, such as those due to bleaching (Matsuda et al., 2020), and may be integral to adaptation to environmental change (Kenkel and Matz, 2016). Further, the expression patterns underlying the tested micro-environmental differences are found to be evolutionary conserved in the distantly-related stony corals *S. pistillata* and *Acropora* spp. Future study of multiple colonies and species will clarify the extent to which the general patterns we observe across the colony studied here are found across differing colony morphologies, diurnal and seasonal cycles, and geographic location. Further, the diversity of gene expression and physiology across a coral colony needs to be taken into account when designing experiments with coral fragments from multiple colonies.

6 Figure Legends

Figure 1. **Micro-environments and responses in sections of an individual coral colony.** Photograph of the *S. pistillata* colony analyzed for physiological and transcriptomic intracolonial differences taken *in situ* (8 m depth) from the east side of the colony (a). Three-dimensional reconstructions of the coral colony showing locations of branches based on cardinal direction (top view, b) and ring height (oblique view, c). Inset in (c) shows branch axis sampling locations at tips, junction, and base per branch.

Figure 2. In-situ water column concentrations of dissolved oxygen (a) and total microbial cells (b) between branches inside and outside *S. pistillata* colonies. Non-metric multidimensional scaling (NMDS) of all expressed genes of the coral host (c) and photosymbiont (d) with factor effects color- and shape-coded. Host ring and branch position-based clusters are significant (Supplementary Table 7) and marked by dashed and solid ellipses, respectively.

Figure 3. **Differential gene expression across coral species and terms clustering in host and symbiont.** Venn diagram (a) representing the proportional counts of shared tip vs. base DE genes in *S. pistillata* (here) and two species of *Acropora* (Hemond et al., 2014) (Supplementary Table

9), with shaded regions representing genes showing the same DE patterns and noting "up" and "down" regulated genes. Enrichment patterns of clustered host KEGG (*S. pistillata*; b) and photosymbiont GO terms (UniProt *S. microadriaticum*; c) across factor comparisons. Host terms enriched in both *S. pistillata* (here) and two species of *Acropora* (Hemond et al., 2014) for tip vs base comparisons, are shown as green text. Hierarchical tree clustering reflects functional similarity between terms. Color-coded heatmap scores equal to $\log_{10}$(adjusted p-value) of enriched terms multiplied by 1 and -1 for up- and down-regulated genes, respectively (for clarity, values <-2 and >2 are shown as 2 and -2).

Figure 4. **Toxicity potential.** Nematocyst abundance (a) and hemolytic units per area (b), and gene expression patterns of putative toxins as $\log_2$FC between branch tips (positive values) and bases (negative values) (c), and $\log_{10}$FPKM along *S. pistillata* branch axis (d). Only significantly DE toxin genes are shown ($p<0.05$). The two most abundant transcripts, a cytolysin annotated as stichotoxin and an uncharacterized gene, for which reciprocal BLAST hits suggest it is a SCRiP (Supplementary14 Table), are noted with a red star (d).

Figure 5. **Skeleton characteristics and biomineralization gene expression.** Microstructural differences of corallites and coenosteal spines along the branch axis (a; tip in i, ii; junction in iii, iv; base in v, vi). Corallite spacing (b) and ellipticity (c) along *S. pistillata* branch axis. Several known biomineralization genes were DE, shown as $\log_2$FC between branch tips (positive values) and bases (negative values) (d) and $\log_{10}$FPKM along the branch axis (e) to clarify genes with high versus low expression. Only significantly DE genes are shown ($p<0.05$).

Figure 6. **Micro-environmental variation across a colony leads to physiological and transcriptional differences.** Schematic of environmental parameters (e.g., flow and light intensity, left) and resulting differential gene expression patterns and physiological outcomes for key processes focusing on those enhanced at branch tips (right). We cannot assign gene expression to specific tissue layers or cell types in most cases, except for the likely localization of toxin and biomineralization genes to the oral ectoderm and calicoderm, respectively.

7 Conflict of Interest

The authors declare that the research was conducted in the absence of any commercial or financial relationships that could be construed as a potential conflict of interest.

8 Author Contribution Statement

YP, OY, DT, DS, and TM conceived the study. YP, OY, ES prepared the samples. JLD, AM, YP, OY, ES, and JS conducted formal analysis of the data. All authors wrote the manuscript and approve of this submission.

9 Funding

This work was supported by grants 1239/13 and 312/15 from the Israel Science Foundation (to DS and TM, respectively) and by the associated grant number 2236/16 from the Israeli National Center for Personalized Medicine (to DS). This work has received funding to TM from the European Research Council under the European Union's Horizon 2020 research and innovation programme (grant agreement No 755876). JLD was supported by the Zuckerman STEM Leadership Program. Computations presented in this work were performed on the Hive

computer cluster at the University of Haifa, which is partly funded by Israel Science Foundation grant 2155/15.

10 Acknowledgements

We thank Yarden Ben-Tabou de-Leon for drawing the summary Figure 6 and Dikla Aharonovich for guidance and laboratory assistance. We thank the Crown Genomics Institute of the Nancy and Stephen Grand Israel National Center for Personalized Medicine, Weizmann Institute of Science for transcriptome sequencing.

11 Data Availability Statement

The data underlying this article are available in the article, in its online Supplementary Material, and on GitHub in the following repository:
https://github.com/jeanadrake/Single_coral_colony_transcriptomes_physiology.

12 References

Akiva, A., Neder, M., Kahil, K., Gavriel, R., Pinkas, I., Goobes, G., and Mass, T. (2018). Minerals in the pre-settled coral *Stylophora pistillata* crystallize via protein and ion changes. *Nature Communications* 9**,** 1880.

Albalat, R. (2012). Evolution of the genetic machinery of the visual cycle: a novelty of the vertebrate eye? *Molecular Biology and Evolution* 29**,** 1461-1469.

Alvarez, C., Mancheno, J.M., Martínez, D., Tejuca, M., Pazos, F., and Lanio, M.E. (2009). Sticholysins, two pore-forming toxins produced by the Caribbean sea anemone *Stichodactyla helianthus*: their interaction with membranes. *Toxicon* 54**,** 1135-1147.

Anthony, K.R., Hoogenboom, M.O., and Connolly, S.R. (2005). Adaptive variation in coral geometry and the optimization of internal colony light climates. *Functional Ecology* 19**,** 17-26.

Aranda, M., Li, Y., Liew, Y.J., Baumgarten, S., Simakov, O., Wilson, M.C., Piel, J., Ashoor, H., Bougouffa, S., and Bajic, V.B. (2016). Genomes of coral dinoflagellate symbionts highlight evolutionary adaptations conducive to a symbiotic lifestyle. *Scientific Reports* 6**,** 1-15.

Bartosz, G., Finkelshtein, A., Przygodzki, T., Bsor, T., Nesher, N., Sher, D., and Zlotkin, E. (2008). A pharmacological solution for a conspecific conflict: ROS-mediated territorial aggression in sea anemones. *Toxicon* 51**,** 1038-1050.

Basulto, A., Pérez, V.M., Noa, Y., Varela, C., Otero, A.J., and Pico, M.C. (2006). Immunohistochemical targeting of sea anemone cytolysins on tentacles, mesenteric filaments and isolated nematocysts of *Stichodactyla helianthus*. *Journal of Experimental Zoology Part A: Comparative Experimental Biology* 305**,** 253-258.

Ben-Ari, H., Paz, M., and Sher, D. (2018). The chemical armament of reef-building corals: inter- and intra-specific variation and the identification of an unusual actinoporin in *Stylophora pistilata*. *Scientific Reports* 8**,** 1-13.

Bertucci, A., Tambutté, S., Supuran, C., Allemand, D., and Zoccola, D. (2011). A new coral carbonic anhydrase in *Stylophora pistillata*. *Marine Biotechnology* 13**,** 992-1002.

Bryant, D.M., Johnson, K., DiTommaso, T., Tickle, T., Couger, M.B., Payzin-Dogru, D., Lee, T.J., Leigh, N.D., Kuo, T.-H., and Davis, F.G. (2017). A tissue-mapped axolotl de novo transcriptome enables identification of limb regeneration factors. *Cell Reports* 18**,** 762-776.

820 Buchfink, B., Xie, C., and Huson, D.H. (2015). Fast and sensitive protein alignment using
821 DIAMOND. *Nature Methods* 12**,** 59-60.
822 Carpenter, L.W., and Patterson, M.R. (2007). Water flow influences the distribution of
823 photosynthetic efficiency within colonies of the scleractinian coral *Montastrea annularis*
824 (Ellis and Solander, 1786); implications for coral bleaching. *Journal of Experimental*
825 *Marine Biology and Ecology* 351**,** 10-26.
826 Cartwright, P., Bowsher, J., and Buss, L.W. (1999). Expression of a Hox gene, Cnox-2, and the
827 division of labor in a colonial hydroid. *Proceedings of the National Academy of Sciences*
828 96**,** 2183-2186.
829 Chang, S., Elkins, C., Alley, M., Eaton, J., and Monismitha, S. (2009). Flow inside a coral
830 colony measured using magnetic resonance velocimetry. *Limnology and Oceanography*
831 54**,** 1819-1827.
832 Chiu, Y.-L., Shikina, S., Yoshioka, Y., Shinzato, C., and Chang, C.-F. (2020). De novo
833 transcriptome assembly from the gonads of a scleractinian coral, *Euphyllia ancora*:
834 molecular mechanisms underlying scleractinian gametogenesis. *BMC Genomics* 21**,** 1-20.
835 Conlan, J.A., Humphrey, C.A., Severati, A., and Francis, D.S. (2018). Intra-colonial diversity in
836 the scleractinian coral, *Acropora millepora*: identifying the nutritional gradients
837 underlying physiological integration and compartmentalised functioning. *PeerJ* 6**,** e4239.
838 Coronado, I., Fine, M., Bosellini, F.R., and Stolarski, J. (2019). Impact of ocean acidification on
839 crystallographic vital effect of the coral skeleton. *Nature Communications* 10**,** 1-9.
840 D'A, M., and Le Tissier, A. (1988). The growth and formation of branch tips of *Pocillopora*
841 *damicornis* (Linnaeus). *Journal of Experimental Marine Biology and Ecology* 124**,** 115-
842 131.
843 Dennison, W.C., and Barnes, D.J. (1988). Effect of water motion on coral photosynthesis and
844 calcification. *Journal of Experimental Marine Biology and Ecology* 115**,** 67-77.
845 DePristo, M.A., Banks, E., Poplin, R., Garimella, K.V., Maguire, J.R., Hartl, C., Philippakis,
846 A.A., Del Angel, G., Rivas, M.A., and Hanna, M. (2011). A framework for variation
847 discovery and genotyping using next-generation DNA sequencing data. *Nature Genetics*
848 43**,** 491.
849 Dobin, A., Davis, C.A., Schlesinger, F., Drenkow, J., Zaleski, C., Jha, S., Batut, P., Chaisson,
850 M., and Gingeras, T.R. (2013). STAR: ultrafast universal RNA-Seq aligner.
851 *Bioinformatics* 29**,** 15-21.
852 Drake, J.L., Mass, T., Haramaty, L., Zelzion, E., Bhattacharya, D., and Falkowski, P.G. (2013).
853 Proteomic analysis of skeletal organic matrix from the stony coral *Stylophora pistillata*.
854 *Proceedings of the National Academy of Sciences* 110**,** 3788-3793.
855 Drake, J.L., Schaller, M.F., Mass, T., Godfrey, L., Fu, A., Sherrell, R.M., Rosenthal, Y., and
856 Falkowski, P.G. (2017). Molecular and geochemical perspectives on the influence of CO_2
857 on calcification in coral cell cultures. *Limnology and Oceanography*.
858 Duffy, D.J., Plickert, G., Kuenzel, T., Tilmann, W., and Frank, U. (2010). Wnt signaling
859 promotes oral but suppresses aboral structures in *Hydractinia* metamorphosis and
860 regeneration. *Development* 137**,** 3057-3066.
861 Falkowski, P.G., Dubinsky, Z., Muscatine, L., and Porter, J.W. (1984). Light and the
862 bioenergetics of a symbiotic coral. *Bioscience* 34**,** 705-709.
863 Fang, L.-S., Chen, Y.-w.J., and Chen, C.-S. (1989). Why does the white tip of stony coral grow
864 so fast without zooxanthellae? *Marine Biology* 103**,** 359-363.

Garren, M., Son, K., Raina, J.-B., Rusconi, R., Menolascina, F., Shapiro, O.H., Tout, J., Bourne, D.G., Seymour, J.R., and Stocker, R. (2014). A bacterial pathogen uses dimethylsulfoniopropionate as a cue to target heat-stressed corals. *The ISME Journal* 8**,** 999-1007.

Gavriel, R., Nadav-Tsubery, M., Glick, Y., Yarmolenko, A., Kofman, R., Keinan-Adamsky, K., Berman, A., Mass, T., and Goobes, G. (2018). The coral protein CARP3 acts from a disordered mineral surface film to divert aragonite crystallization in favor of Mg-calcite. *Advanced Functional Materials* 28**,** 1707321.

Gibbin, E., Gavish, A., Domart-Coulon, I., Kramarsky-Winter, E., Shapiro, O., Meibom, A., and Vardi, A. (2018). Using NanoSIMS coupled with microfluidics to visualize the early stages of coral infection by *Vibrio coralliilyticus*. *BMC microbiology* 18**,** 1-10.

Giese, C., Mebs, D., and Werding, B. (1996). Resistance and vulnerability of crustaceans to cytolytic sea anemone toxins. *Toxicon* 34**,** 955-958.

Gladfelter, E.H., Michel, G., and Sanfelici, A. (1989). Metabolic gradients along a branch of the reef coral *Acropora palmata*. *Bulletin of Marine Science* 44**,** 1166-1173.

Goreau, T.F. (1959). The physiology of skeleton formation in corals. I. A method for measuring the rate of calcium deposition by corals under different conditions. *Biological Bulletin* 116**,** 59-75.

Guillemot, F., and Zimmer, C. (2011). From cradle to grave: the multiple roles of fibroblast growth factors in neural development. *Neuron* 71**,** 574-588.

Gutner-Hoch, E., Ben-Asher, H.W., Yam, R., Shemesh, A., and Levy, O. (2017). Identifying genes and regulatory pathways associated with the scleractinian coral calcification process. *PeerJ* 5**,** e3590.

Helmuth, B.S., Timmerman, B., and Sebens, K. (1997). Interplay of host morphology and symbiont microhabitat in coral aggregations. *Marine Biology* 130**,** 1-10.

Hemond, E.M., Kaluziak, S.T., and Vollmer, S.V. (2014). The genetics of colony form and function in Caribbean *Acropora* corals. *BMC Genomics* 15**,** 1133.

Hemond, E.M., and Vollmer, S.V. (2015). Diurnal and nocturnal transcriptomic variation in the Caribbean staghorn coral, *Acropora cervicornis*. *Molecular Ecology* 24**,** 4460-4473.

Hoegh-Guldberg, O., Jacob, D., Taylor, M., Bolaños, T.G., Bindi, M., Brown, S., Camilloni, I., Diedhiou, A., Djalante, R., and Ebi, K. (2019). The human imperative of stabilizing global climate change at 1.5° C. *Science* 365**,** eaaw6974.

Hossain, M.M., and Staples, A.E. (2020). Mass transport and turbulent statistics within two branching coral colonies. *Fluids* 5**,** 153.

Hughes, T.P. (1994). Catastrophes, phase shifts, and large-scale degradation of a Caribbean coral reef. *Science* 265**,** 1547-1551.

Jouiaei, M., Sunagar, K., Federman Gross, A., Scheib, H., Alewood, P.F., Moran, Y., and Fry, B.G. (2015). Evolution of an ancient venom: recognition of a novel family of cnidarian toxins and the common evolutionary origin of sodium and potassium neurotoxins in sea anemone. *Molecular Biology and Evolution* 32**,** 1598-1610.

Kaniewska, P., Anthony, K.R., and Hoegh-Guldberg, O. (2008). Variation in colony geometry modulates internal light levels in branching corals, *Acropora humilis* and *Stylophora pistillata*. *Marine Biology* 155**,** 649-660.

Kaniewska, P., Magnusson, S.H., Anthony, K.R., Reef, R., Kühl, M., and Hoegh-Guldberg, O. (2011). Importance of macro- versus microstructure in modulating light levels inside coral colonies. *Journal of Phycology* 47**,** 846-860.

Kemp, D.W., Hernandez-Pech, X., Iglesias-Prieto, R., Fitt, W.K., and Schmidt, G.W. (2014). Community dynamics and physiology of Symbiodinium spp. before, during, and after a coral bleaching event. *Limnology and Oceanography* 59**,** 788-797.

Kenkel, C.D., and Matz, M.V. (2016). Gene expression plasticity as a mechanism of coral adaptation to a variable environment. *Nature Ecology & Evolution* 1**,** 1-6.

Knowlton, N., Brainard, R.E., Fisher, R., Moews, M., Plaisance, L., and Caley, M.J. (2010). Coral reef biodiversity. *Life in the world's oceans: diversity distribution and abundance***,** 65-74.

Kopp, C., Domart-Coulon, I., Escrig, S., Humbel, B.M., Hignette, M., and Meibom, A. (2015). Subcellular investigation of photosynthesis-driven carbon assimilation in the symbiotic reef coral *Pocillopora damicornis*. *MBio* 6.

Lahn, B.T., and Page, D.C. (1999). Retroposition of autosomal mRNA yielded testis-specific gene family on human Y chromosome. *Nature Genetics* 21**,** 429-433.

Laipnik, R.a., Bissi, V., Sun, C.-Y., Falini, G., Gilbert, P.U., and Mass, T. (2020). Coral acid rich protein selects vaterite polymorph in vitro. *Journal of Structural Biology* 209**,** 107431.

LaJeunesse, T.C., Parkinson, J.E., Gabrielson, P.W., Jeong, H.J., Reimer, J.D., Voolstra, C.R., and Santos, S.R. (2018). Systematic revision of Symbiodiniaceae highlights the antiquity and diversity of coral endosymbionts. *Current Biology* 28**,** 2570-2580. e2576.

Lee, P.N., Pang, K., Matus, D.Q., and Martindale, M.Q. (2006). A WNT of things to come: evolution of Wnt signaling and polarity in cnidarians. *Seminars in Cell & Developmental Biology* 17**,** 157-167.

Liew, Y.J., Aranda, M., and Voolstra, C.R. (2016). Reefgenomics.org - a repository for marine genomics data. *Database* 2016.

Liew, Y.J., Howells, E.J., Wang, X., Michell, C.T., Burt, J.A., Idaghdour, Y., and Aranda, M. (2020). Intergenerational epigenetic inheritance in reef-building corals. *Nature Climate Change* 10**,** 254-259.

Love, M.I., Huber, W., and Anders, S. (2014). Moderated estimation of fold change and dispersion for RNA-Seq data with DESeq2. *Genome Biology* 15**,** 1-21.

Mackie, G. (1986). From aggregates to integrates: physiological aspects of modularity in colonial animals. *Philosophical Transactions of the Royal Society of London. B, Biological Sciences* 313**,** 175-196.

Malik, A., Einbinder, S., Martinez, S., Tchernov, D., Haviv, S., Almuly, R., Zaslansky, P., Polishchuk, I., Pokroy, B., and Stolarski, J. (2021). Molecular and skeletal fingerprints of scleractinian coral biomineralization: from the sea surface to mesophotic depths. *Acta Biomaterialia* 120**,** 263-276.

Marsh Jr, J.A. (1970). Primary productivity of reef-building calcareous red algae. *Ecology* 51**,** 255-263.

Martinez, S., Kolodny, Y., Shemesh, E., Scucchia, F., Nevo, R., Levin-Zaidman, S., Paltiel, Y., Keren, N., Tchernov, D., and Mass, T. (2020). Energy sources of the depth-generalist mixotrophic coral *Stylophora pistillata*. *Frontiers in Marine Science* 7**,** 988.

Mass, T., Brickner, I., Hendy, E., and Genin, A. (2011). Enduring physiological and reproductive benefits of enhanced flow for a stony coral. *Limnology and Oceanography* 56**,** 2176-2188.

Mass, T., Drake, Jeana L., Haramaty, L., Kim, J.D., Zelzion, E., Bhattacharya, D., and Falkowski, Paul G. (2013). Cloning and characterization of four novel coral acid-rich proteins that precipitate carbonates in vitro. *Current Biology* 23**,** 1126-1131.

957 Mass, T., Drake, J.L., Peters, E.C., Jiang, W., and Falkowski, P.G. (2014). Immunolocalization
958 of skeletal matrix proteins in tissue and mineral of the coral *Stylophora pistillata*.
959 *Proceedings of the National Academy of Sciences* 111**,** 12728-12733.
960 Mass, T., Einbinder, S., Brokovich, E., Shashar, N., Vago, R., Erez, J., and Dubinsky, Z. (2007).
961 Photoacclimation of *Stylophora pistillata* to light extremes: metabolism and calcification.
962 *Marine Ecology Progress Series* 334**,** 93-102.
963 Mass, T., Genin, A., Shavit, U., Grinstein, M., and Tchernov, D. (2010). Flow enhances
964 photosynthesis in marine benthic autotrophs by increasing the efflux of oxygen from the
965 organism to the water. *Proceedings of the National Academy of Sciences* 107**,** 2527-2531.
966 Mass, T., Putnam, H.M., Drake, J.L., Zelzion, E., Gates, R.D., Bhattacharya, D., and Falkowski,
967 P.G. (2016). Temporal and spatial expression patterns of biomineralization proteins
968 during early development in the stony coral *Pocillopora damicornis*. *Proceedings of the*
969 *Royal Society B: Biological Sciences* 283**,** 20160322.
970 Matsuda, S.B., Huffmyer, A.S., Lenz, E.A., Davidson, J.M., Hancock, J.R., Przybylowski, A.,
971 Innis, T., Gates, R.D., and Barott, K.L. (2020). Coral bleaching susceptibility Is
972 predictive of subsequent mortality within but not between coral species. *Frontiers in*
973 *Ecology and Evolution* 8.
974 Meesters, E.H., and Bak, R.P. (1995). Age-related deterioration of a physiological function in the
975 branching coral *Acropora palmata*. *Marine Ecology Progress Series* 121**,** 203-209.
976 Mummadisetti, M.P., Drake, J.L., and Falkowski, P.G. (2021). The spatial network of skeletal
977 proteins in a stony coral. *Journal of The Royal Society Interface* 18**,** 20200859.
978 Nakamura, H., Asari, T., Ohizumi, Y., Kobayashi, J.i., Yamasu, T., and Murai, A. (1993).
979 Isolation of zooxanthellatoxins, novel vasoconstrictive substances from the zooxanthella
980 *Symbiodinium* sp. *Toxicon* 31**,** 371-376.
981 Palumbi, S.R., Barshis, D.J., Traylor-Knowles, N., and Bay, R.A. (2014). Mechanisms of reef
982 coral resistance to future climate change. *Science* 344**,** 895-898.
983 Park, E., Hwang, D.-S., Lee, J.-S., Song, J.-I., Seo, T.-K., and Won, Y.-J. (2012). Estimation of
984 divergence times in cnidarian evolution based on mitochondrial protein-coding genes and
985 the fossil record. *Molecular Phylogenetics and Evolution* 62**,** 329-345.
986 Peled, Y., Drake, J.L., Malik, A., Almuly, R., Lalzar, M., Morgenstern, D., and Mass, T. (2020).
987 Optimization of skeletal protein preparation for LC–MS/MS sequencing yields additional
988 coral skeletal proteins in *Stylophora pistillata*. *BMC Materials* 2**,** 8.
989 Primor, N., and Zlotkin, E. (1975). On the ichthyotoxic and hemolytic action of the skin
990 secretion of the flatfish *Pardachirus marmoratus* (Soleidae). *Toxicon* 13**,** 227-231.
991 Puverel, S., Tambutté, E., Pereira-Mouries, L., Zoccola, D., Allemand, D., and Tambutté, S.
992 (2005). Soluble organic matrix of two Scleractinian corals: Partial and comparative
993 analysis. *Comparative Biochemistry and Physiology Part B* 141**,** 480-487.
994 Rachamim, T., Morgenstern, D., Aharonovich, D., Brekhman, V., Lotan, T., and Sher, D. (2015).
995 The dynamically evolving nematocyst content of an anthozoan, a scyphozoan, and a
996 hydrozoan. *Molecular Biology and Evolution* 32**,** 740-753.
997 Ralph, P., Gademann, R., Larkum, A., and Kühl, M. (2002). Spatial heterogeneity in active
998 chlorophyll fluorescence and PSII activity of coral tissues. *Marine Biology* 141**,** 639-646.
999 Ramos-Silva, P., Kaandorp, J., Huisman, L., Marie, B., Zanella-Cleon, I., Guichard, N., Miller,
1000 D.J., and Marin, F. (2013). The skeletal proteome of the coral *Acropora millepora*: The
1001 evolution of calcification by cooption and domain shuffling. *Molecular Biology and*
1002 *Evolution*.

1003 Reinhardt, B., Broun, M., Blitz, I.L., and Bode, H.R. (2004). HyBMP5-8b, a BMP5-8
1004 orthologue, acts during axial patterning and tentacle formation in *Hydra*. *Developmental*
1005 *Biology* 267**,** 43-59.
1006 Rinkevich, B., and Loya, Y. (1983). Oriented translocation of energy in grafted reef corals.
1007 *Coral Reefs* 1**,** 243-247.
1008 Ritchie, K.B. (2006). Regulation of microbial populations by coral surface mucus and mucus-
1009 associated bacteria. *Marine Ecology Progress Series* 322**,** 1-14.
1010 Ritchie, R. (2008). Universal chlorophyll equations for estimating chlorophylls a, b, c, and d and
1011 total chlorophylls in natural assemblages of photosynthetic organisms using acetone,
1012 methanol, or ethanol solvents. *Photosynthetica* 46**,** 115-126.
1013 Rocha, R.J., Silva, A.M., Fernandes, M.H.V., Cruz, I.C., Rosa, R., and Calado, R. (2014).
1014 Contrasting light spectra constrain the macro and microstructures of scleractinian corals.
1015 *PLOS ONE* 9.
1016 Rueffler, C., Hermisson, J., and Wagner, G.P. (2012). Evolution of functional specialization and
1017 division of labor. *Proceedings of the National Academy of Sciences* 109**,** E326-E335.
1018 Schiller, C., and Herndl, G.J. (1989). Evidence of enhanced microbial activity in the interstitial
1019 space of branched corals: possible implications for coral metabolism. *Coral Reefs* 7**,** 179-
1020 184.
1021 Schmidt, C.A., Daly, N.L., and Wilson, D.T. (2019). Coral venom toxins. *Frontiers in Ecology*
1022 *and Evolution* 7**,** 320.
1023 Schmidt-Roach, S., Miller, K.J., Lundgren, P., and Andreakis, N. (2014). With eyes wide open: a
1024 revision of species within and closely related to the *Pocillopora damicornis* species
1025 complex (Scleractinia; Pocilloporidae) using morphology and genetics. *Zoological*
1026 *Journal of the Linnean Society* 170**,** 1-33.
1027 Sebens, K.P., Witting, J., and Helmuth, B. (1997). Effects of water flow and branch spacing on
1028 particle capture by the reef coral *Madracis mirabilis* (Duchassaing and Michelotti).
1029 *Journal of Experimental Marine Biology and Ecology* 211**,** 1-28.
1030 Sergushichev, A.A. (2016). An algorithm for fast preranked gene set enrichment analysis using
1031 cumulative statistic calculation. *BioRxiv***,** 060012.
1032 Shenkar, N., Fine, M., and Loya, Y. (2005). Size matters: bleaching dynamics of the coral
1033 *Oculina patagonica*. *Marine Ecology Progress Series* 294**,** 181-188.
1034 Siegfried, E., and Perrimon, N. (1994). *Drosophila* wingless: a paradigm for the function and
1035 mechanism of Wnt signaling. *Bioessays* 16**,** 395-404.
1036 Steinmetz, P.R. (2019). A non-bilaterian perspective on the development and evolution of animal
1037 digestive systems. *Cell and Tissue Research* 377**,** 321-339.
1038 Stimson, J. (1978). Mode and timing of reproduction in some common hermatypic corals of
1039 Hawaii and Enewetak. *Marine Biology* 48**,** 173-184.
1040 Subramanian, A., Tamayo, P., Mootha, V.K., Mukherjee, S., Ebert, B.L., Gillette, M.A.,
1041 Paulovich, A., Pomeroy, S.L., Golub, T.R., and Lander, E.S. (2005). Gene set enrichment
1042 analysis: a knowledge-based approach for interpreting genome-wide expression profiles.
1043 *Proceedings of the National Academy of Sciences* 102**,** 15545-15550.
1044 Sunagawa, S., DeSalvo, M.K., Voolstra, C.R., Reyes-Bermudez, A., and Medina, M. (2009).
1045 Identification and gene expression analysis of a taxonomically restricted cysteine-rich
1046 protein family in reef-building corals. *PLOS ONE* 4**,** e4865.

1047 Surekha, K.L., Khade, S., Trimbake, D., Patwardhan, R., Nadimpalli, S.K., and Ghaskadbi, S.
1048 (2020). Differential expression of BMP inhibitors gremlin and noggin in *Hydra* suggests
1049 distinct roles during budding and patterning of tentacles. *Developmental Dynamics*.
1050 Takeuchi, T., Yamada, L., Shinzato, C., Sawada, H., and Satoh, N. (2016). Stepwise evolution of
1051 coral biomineralization revealed with genome-wide proteomics and transcriptomics.
1052 *PLOS ONE* 11**,** e0156424.
1053 RStudio Team. (2019). "RStudio: Integrated Development for R". (Boston, MA: RStudio, Inc.).
1054 Voolstra, C.R., Li, Y., Liew, Y.J., Baumgarten, S., Zoccola, D., Flot, J.-F., Tambutté, S.,
1055 Allemand, D., and Aranda, M. (2017). Comparative analysis of the genomes of
1056 *Stylophora pistillata* and *Acropora digitifera* provides evidence for extensive differences
1057 between species of corals. *Scientific Reports* 7**,** 17583.
1058 Walden, P.D., and Cowan, N.J. (1993). A novel 205-kilodalton testis-specific serine/threonine
1059 protein kinase associated with microtubules of the spermatid manchette. *Molecular and*
1060 *Cellular Biology* 13**,** 7625-7635.
1061 Wallace, C.C. (1978). The coral genus *Acropora* (scleractinia: Astrocoaniina: Acroporidae) in
1062 the central and southern Great Barrier Reef province. *Memoires of the Queensland*
1063 *Museum* 18**,** 273-319.
1064 Wallace, C.C. (1985). Reproduction, recruitment and fragmentation in nine sympatric species of
1065 the coral genus *Acropora*. *Marine Biology* 88**,** 217-233.
1066 Wangpraseurt, D., Polerecky, L., Larkum, A.W., Ralph, P.J., Nielsen, D.A., Pernice, M., and
1067 Kühl, M. (2014). The in situ light microenvironment of corals. *Limnology and*
1068 *Oceanography* 59**,** 917-926.
1069 Winkler, R., Antonius, A., and Abigail Renegar, D. (2004). The skeleton eroding band disease
1070 on coral reefs of Aqaba, Red Sea. *Marine Ecology* 25**,** 129-144.
1071 Xu, X., Weinstein, M., Li, C., and Deng, C.-X. (1999). Fibroblast growth factor receptors
1072 (FGFRs) and their roles in limb development. *Cell and Tissue Research* 296**,** 33-43.
1073 Yahel, R., Yahel, G., Berman, T., Jaffe, J.S., and Genin, A. (2005). Diel pattern with abrupt
1074 crepuscular changes of zooplankton over a coral reef. *Limnology and Oceanography* 50**,**
1075 930-944.
1076 Yosef, O., Popovits, Y., Malik, A., Ofek-Lalzer, M., Mass, T., and Sher, D. (2020). A tentacle
1077 for every occasion: comparing the hunting tentacles and sweeper tentacles, used for
1078 territorial competition, in the coral *Galaxea fascicularis*. *BMC Genomics* 21**,** 1-16.
1079 Young, M.D., Wakefield, M.J., Smyth, G.K., and Oshlack, A. (2012). goseq: Gene Ontology
1080 testing for RNA-seq datasets. *R Bioconductor* 8**,** 1-25.
1081 Yu, G., Lam, T.T.-Y., Zhu, H., and Guan, Y. (2018). Two methods for mapping and visualizing
1082 associated data on phylogeny using ggtree. *Molecular Biology and Evolution* 35**,** 3041-
1083 3043.
1084 Zaquin, T., Malik, A., Drake, J.L., Putnam, H.M., and Mass, T. (2021). Evolution of protein-
1085 mediated biomineralization in scleractinian corals. *Frontiers in Genetics* 12**,** 52.
1086 Zoccola, D., Ganot, P., Bertucci, A., Caminiti-Segonds, N., Techer, N., Voolstra, C.R., Aranda,
1087 M., Tambutté, E., Allemand, D., and Casey, J.R. (2015). Bicarbonate transporters in
1088 corals point towards a key step in the evolution of cnidarian calcification. *Scientific*
1089 *Reports* 5.
1090 Zoccola, D., Innocenti, A., Bertucci, A., Tambutté, E., Supuran, C.T., and Tambutté, S. (2016).
1091 Coral carbonic anhydrases: regulation by ocean acidification. *Marine Drugs* 14**,** 109.
1092

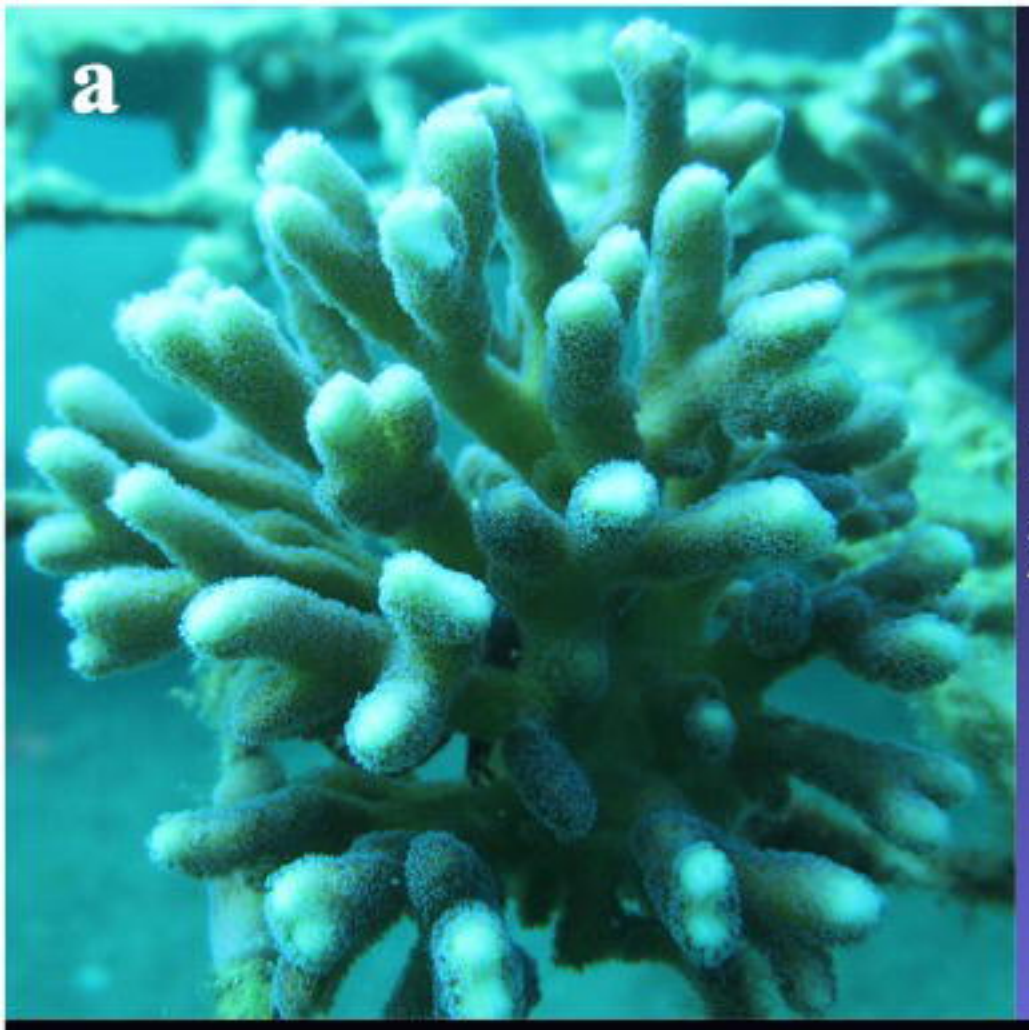
a

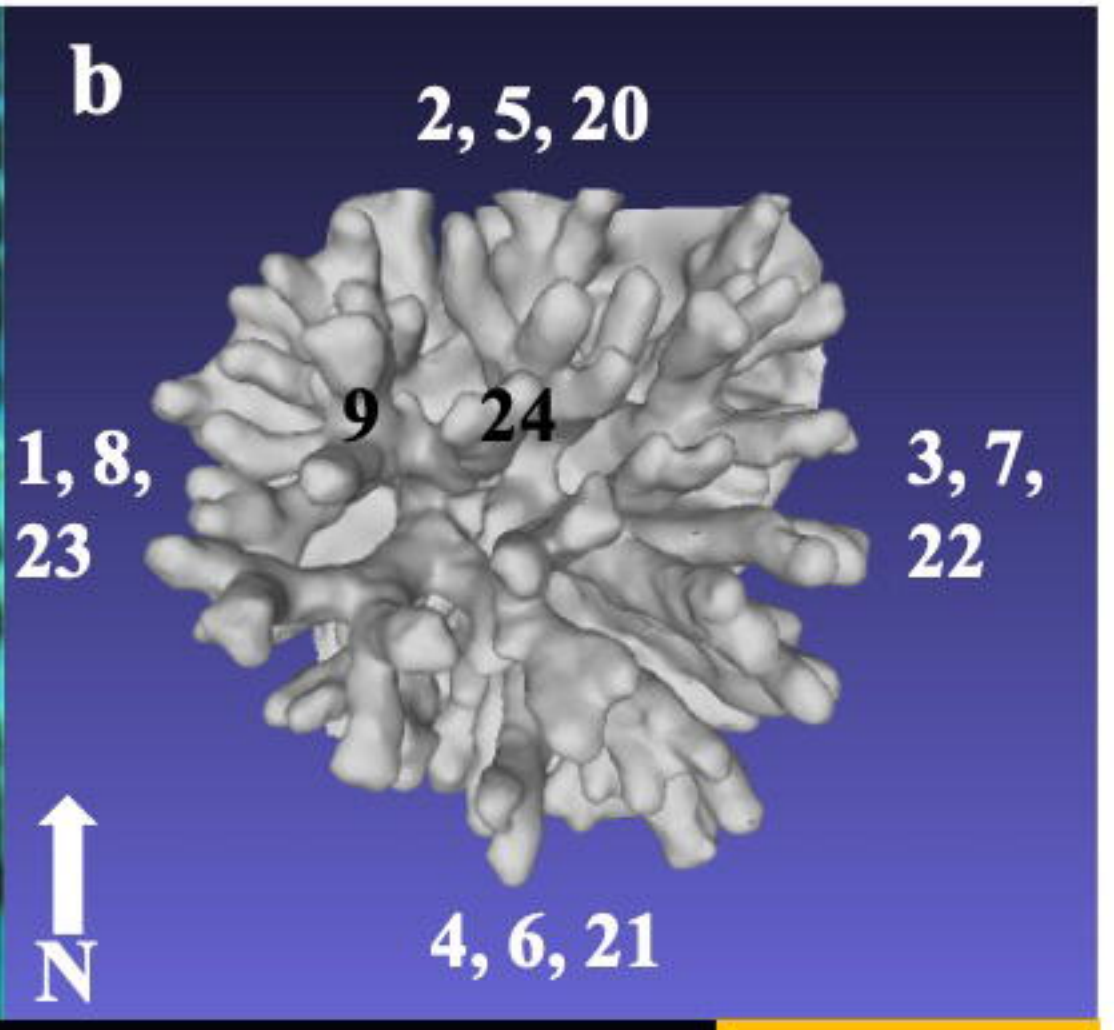
b
2, 5, 20
9
24
1, 8,
23
3, 7,
22
N
4, 6, 21

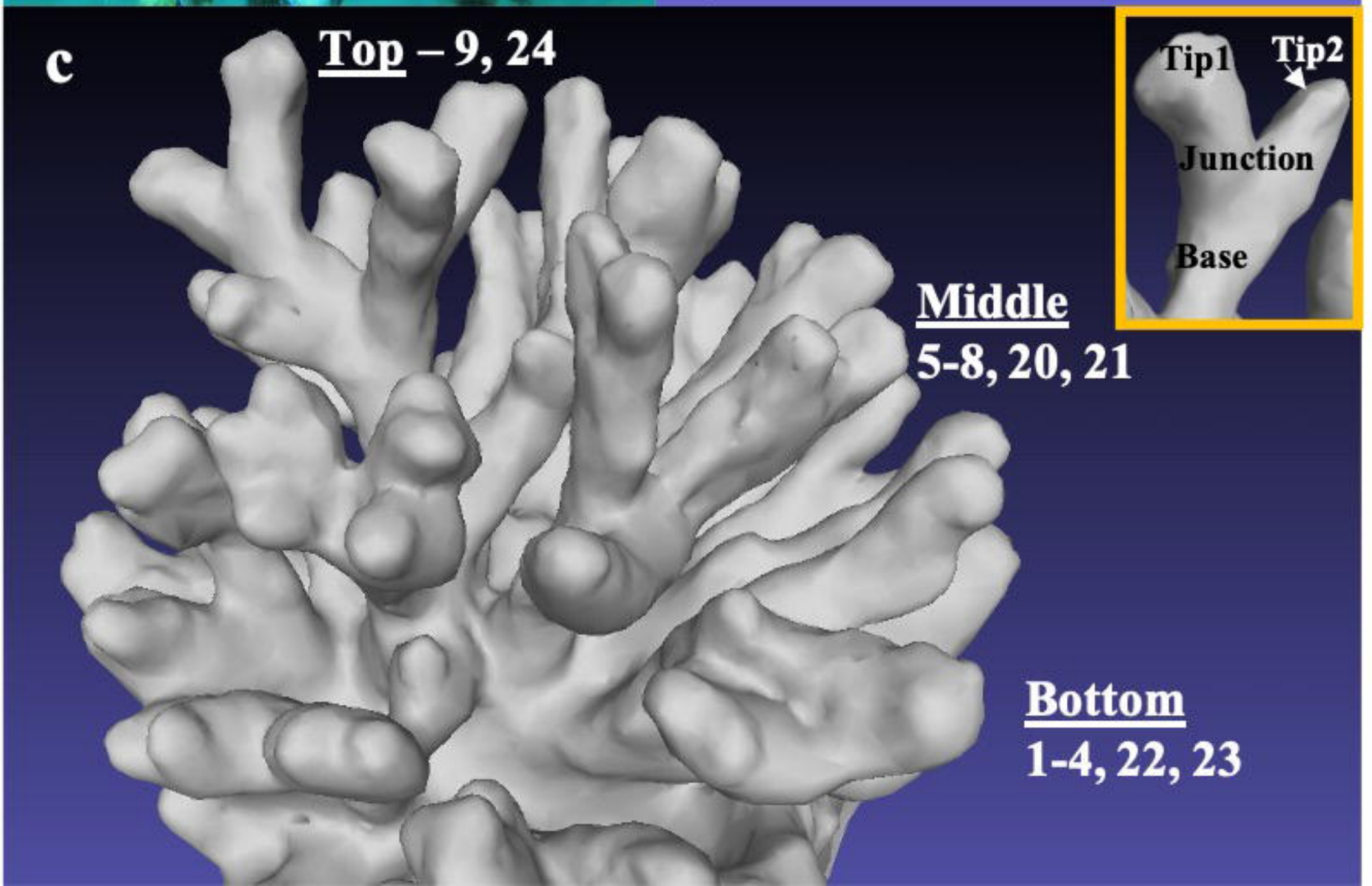
c
Top – 9, 24
Tip1
Tip2
Junction
Base
Middle
5-8, 20, 21
Bottom
1-4, 22, 23

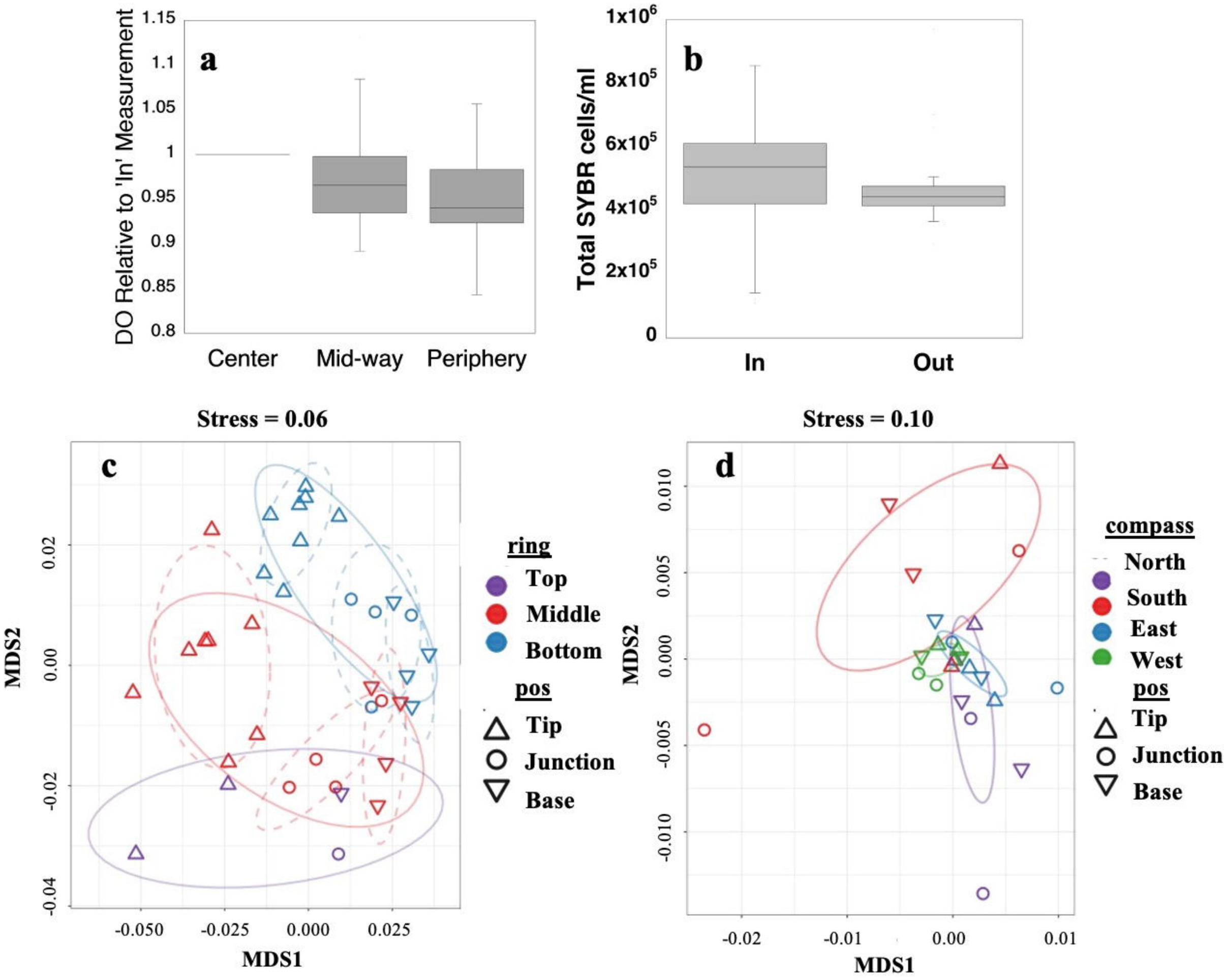
a
DO Relative to 'In' Measurement
1.15
1.1
1.05
1
0.95
0.9
0.85
0.8
Center
Mid-way
Periphery
b
Total SYBR cells/ml
1x10^6
8x10^5
6x10^5
4x10^5
2x10^5
0
In
Out
Stress = 0.06
c
MDS2
0.02
0.00
-0.02
-0.04
-0.050
-0.025
0.000
0.025
MDS1
ring
Top
Middle
Bottom
pos
Tip
Junction
Base
Stress = 0.10
d
MDS2
0.010
0.005
0.000
-0.005
-0.010
-0.02
-0.01
0.00
0.01
MDS1
compass
North
South
East
West
pos
Tip
Junction
Base

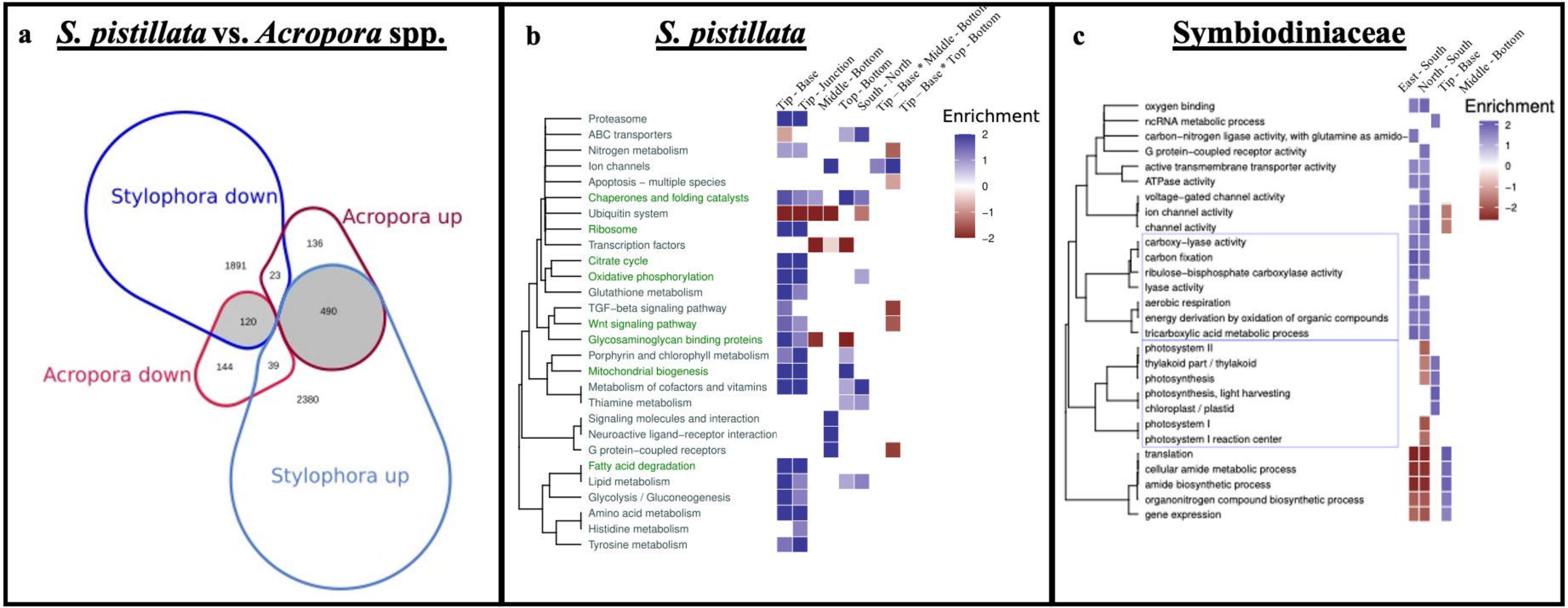
a
S. pistillata vs. Acropora spp.
Stylophora down
Acropora up
Acropora down
Stylophora up
1891
136
23
120
490
144
39
2380
b
S. pistillata
Tip - Base
Tip - Junction
Middle - Bottom
Top - Bottom
South - North
Tip – Base * Middle - Bottom
Tip – Base * Top - Bottom
Enrichment
2
1
0
−1
−2
Proteasome
ABC transporters
Nitrogen metabolism
Ion channels
Apoptosis – multiple species
Chaperones and folding catalysts
Ubiquitin system
Ribosome
Transcription factors
Citrate cycle
Oxidative phosphorylation
Glutathione metabolism
TGF−beta signaling pathway
Wnt signaling pathway
Glycosaminoglycan binding proteins
Porphyrin and chlorophyll metabolism
Mitochondrial biogenesis
Metabolism of cofactors and vitamins
Thiamine metabolism
Signaling molecules and interaction
Neuroactive ligand−receptor interaction
G protein−coupled receptors
Fatty acid degradation
Lipid metabolism
Glycolysis / Gluconeogenesis
Amino acid metabolism
Histidine metabolism
Tyrosine metabolism
c
Symbiodiniaceae
East - South
North - South
Tip - Base
Middle - Bottom
Enrichment
2
1
0
−1
−2
oxygen binding
ncRNA metabolic process
carbon−nitrogen ligase activity, with glutamine as amido−
G protein−coupled receptor activity
active transmembrane transporter activity
ATPase activity
voltage−gated channel activity
ion channel activity
channel activity
carboxy−lyase activity
carbon fixation
ribulose−bisphosphate carboxylase activity
lyase activity
aerobic respiration
energy derivation by oxidation of organic compounds
tricarboxylic acid metabolic process
photosystem II
thylakoid part / thylakoid
photosynthesis
photosynthesis, light harvesting
chloroplast / plastid
photosystem I
photosystem I reaction center
translation
cellular amide metabolic process
amide biosynthetic process
organonitrogen compound biosynthetic process
gene expression

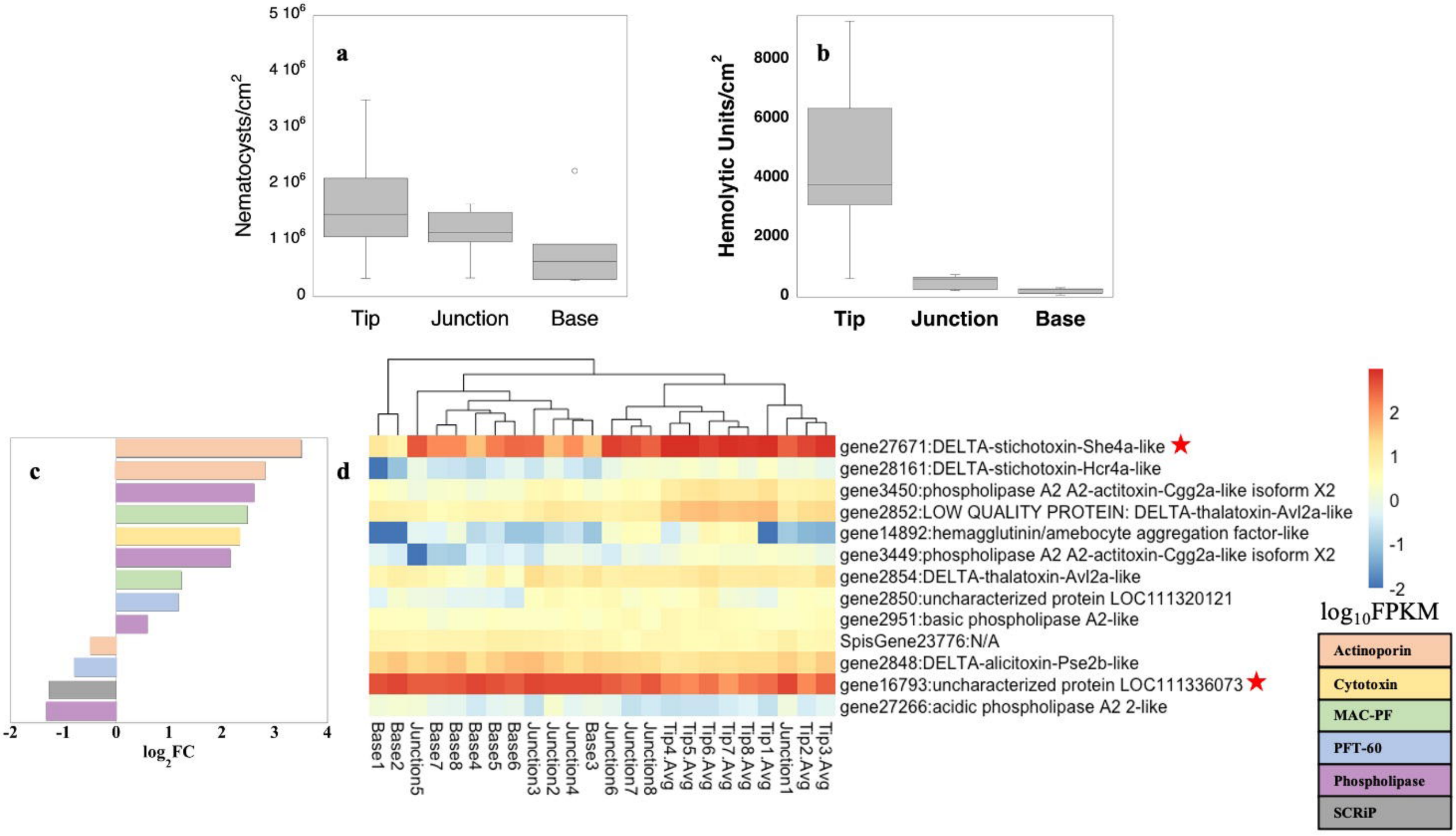
a
Nematocysts/cm2
5 10^6
4 10^6
3 10^6
2 10^6
1 10^6
0
Tip
Junction
Base
b
Hemolytic Units/cm2
8000
6000
4000
2000
0
Tip
Junction
Base
c
-2
-1
0
1
2
3
4
log2FC
d
gene27671:DELTA-stichotoxin-She4a-like
gene28161:DELTA-stichotoxin-Hcr4a-like
gene3450:phospholipase A2 A2-actitoxin-Cgg2a-like isoform X2
gene2852:LOW QUALITY PROTEIN: DELTA-thalatoxin-Avl2a-like
gene14892:hemagglutinin/amebocyte aggregation factor-like
gene3449:phospholipase A2 A2-actitoxin-Cgg2a-like isoform X2
gene2854:DELTA-thalatoxin-Avl2a-like
gene2850:uncharacterized protein LOC111320121
gene2951:basic phospholipase A2-like
SpisGene23776:N/A
gene2848:DELTA-alicitoxin-Pse2b-like
gene16793:uncharacterized protein LOC111336073
gene27266:acidic phospholipase A2 2-like
Base1
Base2
Junction5
Base7
Base8
Base4
Base5
Base6
Junction3
Junction2
Junction4
Base3
Junction6
Junction7
Junction8
Tip4.Avg
Tip5.Avg
Tip6.Avg
Tip7.Avg
Tip8.Avg
Tip1.Avg
Junction1
Tip2.Avg
Tip3.Avg
2
1
0
-1
-2
log10FPKM
Actinoporin
Cytotoxin
MAC-PF
PFT-60
Phospholipase
SCRiP

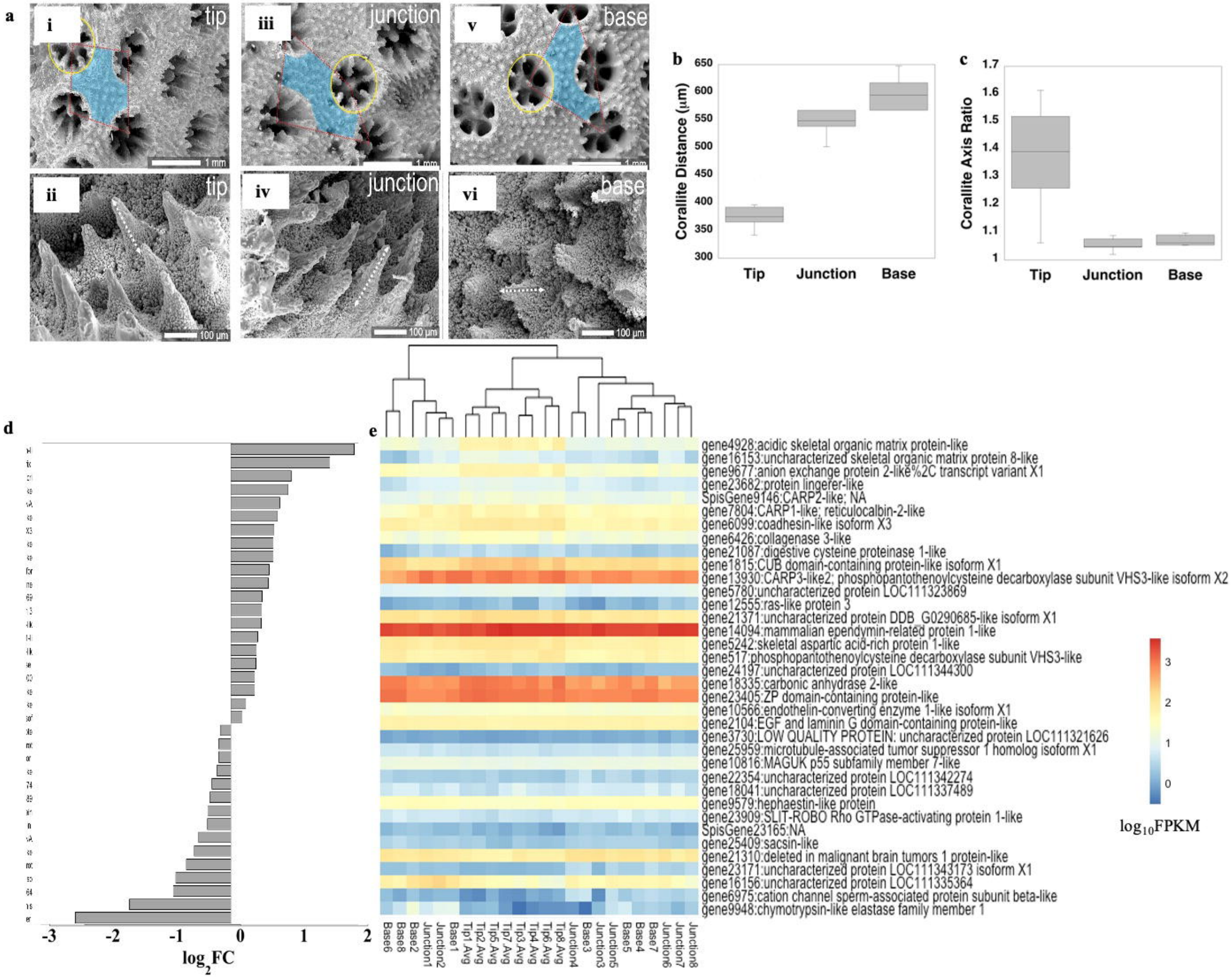
a
i
tip
1 mm
iii
junction
1 mm
v
base
1 mm
ii
tip
100 µm
iv
junction
100 µm
vi
base
100 µm
b
Corallite Distance (µm)
650
600
550
500
450
400
350
300
Tip
Junction
Base
c
Corallite Axis Ratio
1.7
1.6
1.5
1.4
1.3
1.2
1.1
1
Tip
Junction
Base
d
-3
-2
-1
0
1
2
log2FC
e
gene4928:acidic skeletal organic matrix protein-like
gene16153:uncharacterized skeletal organic matrix protein 8-like
gene9677:anion exchange protein 2-like%2C transcript variant X1
gene23682:protein lingerer-like
SpisGene9146:CARP2-like; NA
gene7804:CARP1-like; reticulocalbin-2-like
gene6099:coadhesin-like isoform X3
gene6426:collagenase 3-like
gene21087:digestive cysteine proteinase 1-like
gene1815:CUB domain-containing protein-like isoform X1
gene13930:CARP3-like2; phosphopantothenoylcysteine decarboxylase subunit VHS3-like isoform X2
gene5780:uncharacterized protein LOC111323869
gene12555:ras-like protein 3
gene21371:uncharacterized protein DDB_G0290685-like isoform X1
gene14094:mammalian ependymin-related protein 1-like
gene5242:skeletal aspartic acid-rich protein 1-like
gene517:phosphopantothenoylcysteine decarboxylase subunit VHS3-like
gene24197:uncharacterized protein LOC111344300
gene18335:carbonic anhydrase 2-like
gene23405:ZP domain-containing protein-like
gene10566:endothelin-converting enzyme 1-like isoform X1
gene2104:EGF and laminin G domain-containing protein-like
gene3730:LOW QUALITY PROTEIN: uncharacterized protein LOC111321626
gene25959:microtubule-associated tumor suppressor 1 homolog isoform X1
gene10816:MAGUK p55 subfamily member 7-like
gene22354:uncharacterized protein LOC111342274
gene18041:uncharacterized protein LOC111337489
gene9579:hephaestin-like protein
gene23909:SLIT-ROBO Rho GTPase-activating protein 1-like
SpisGene23165:NA
gene25409:sacsin-like
gene21310:deleted in malignant brain tumors 1 protein-like
gene23171:uncharacterized protein LOC111343173 isoform X1
gene16156:uncharacterized protein LOC111335364
gene6975:cation channel sperm-associated protein subunit beta-like
gene9948:chymotrypsin-like elastase family member 1
Base6
Base8
Base2
Junction1
Junction2
Base1
Tip1.Avg
Tip2.Avg
Tip5.Avg
Tip7.Avg
Tip3.Avg
Tip4.Avg
Tip6.Avg
Tip8.Avg
Junction4
Base3
Junction3
Junction5
Base5
Base4
Base7
Junction6
Junction7
Junction8
3
2
1
0
log10FPKM

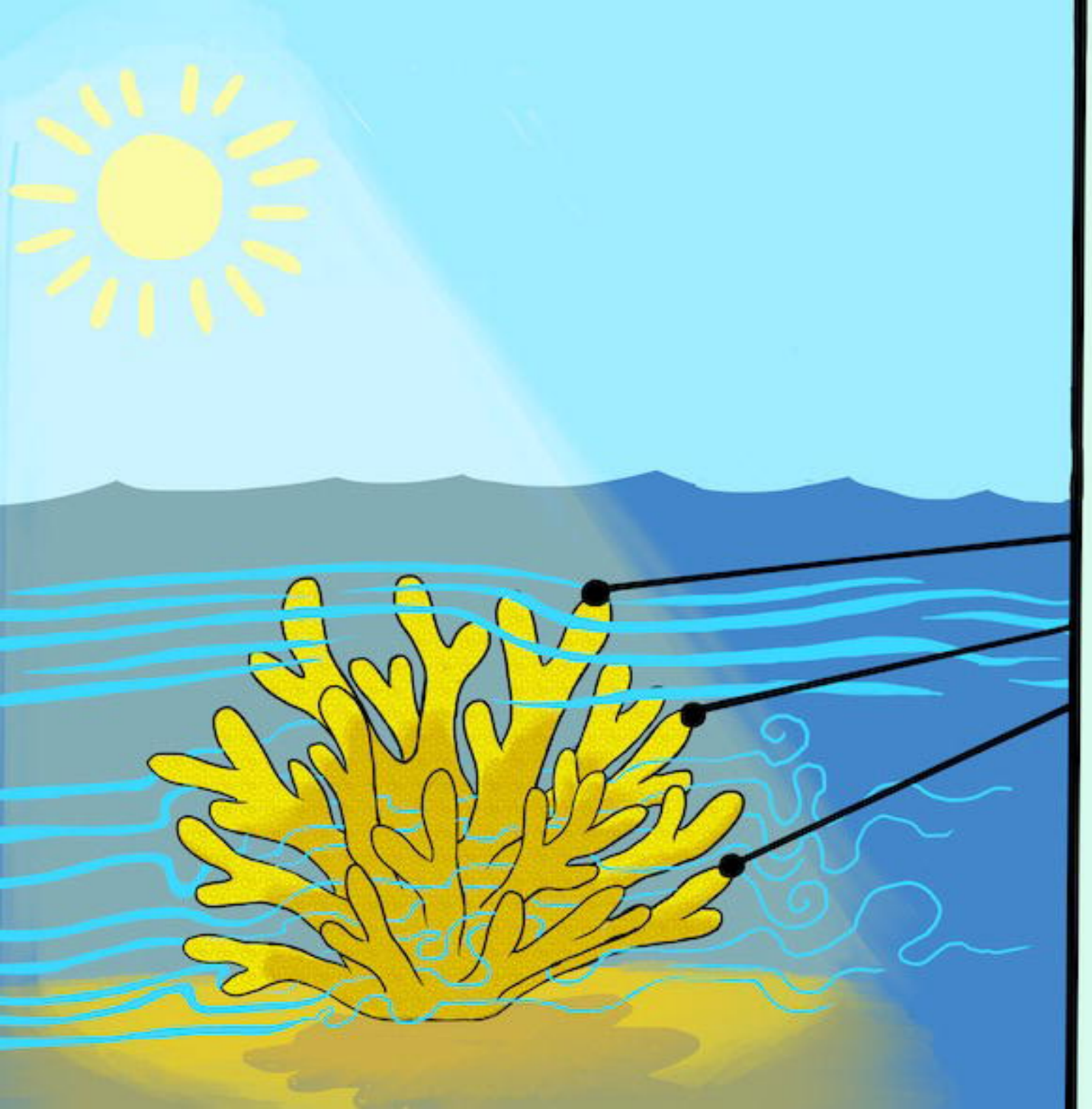

Biomineralization

Hemolytic Toxins

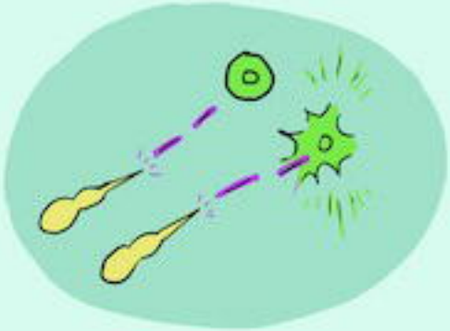

Energy Production

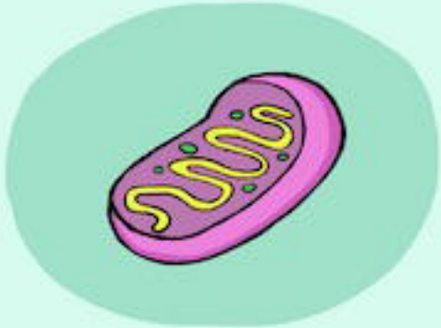

Protein synthesis and folding

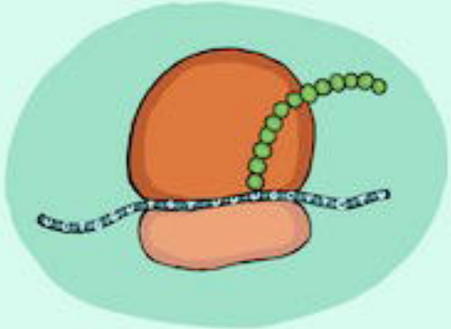

Fatty acid degradation
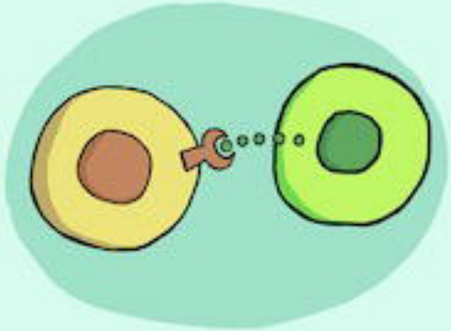
WNT signaling